



1 **Influence of anthropogenic emissions and boundary conditions on multi-model**
2 **simulations of major air pollutants over Europe and North America in the framework**
3 **of AQMEII3**

4 Ulas Im¹, Jesper Heile Christensen¹, Camilla Geels¹, Kaj Mantzius Hansen¹, Jørgen Brandt¹,
5 Efisio Solazzo², Ummugulsum Alyuz³, Alessandra Balzarini⁴, Rocio Baro^{5,a}, Roberto
6 Bellasio⁶, Roberto Bianconi⁶, Johannes Bieser⁷, Augustin Colette⁸, Gabriele Curci^{9,10}, Aidan
7 Farrow¹¹, Johannes Flemming¹², Andrea Fraser¹³, Pedro Jimenez-Guerrero⁵, Nutthida
8 Kitwiroon¹⁴, Peng Liu¹⁵, Uarporn Nopmongkol¹⁶, Laura Palacios-Peña⁵, Guido Pirovano⁴,
9 Luca Pozzoli², Marje Prank^{17,18}, Rebecca Rose¹³, Ranjeet Sokhi¹¹, Paolo Tuccella^{9,10}, Alper
10 Unal³, Marta G. Vivanco^{8,19}, Greg Yarwood¹⁶, Christian Hogrefe²⁰, Stefano Galmarini²

11 ¹ Aarhus University, Department of Environmental Science, Frederiksborgevej 399, DK-4000,
12 Roskilde, Denmark.

13 ² European Commission, Joint Research Centre (JRC), Ispra (VA), Italy.

14 ³ Eurasia Institute of Earth Sciences, Istanbul Technical University, Istanbul, Turkey.

15 ⁴ Ricerca sul Sistema Energetico (RSE SpA), Milan, Italy.

16 ⁵ University of Murcia, Department of Physics, Physics of the Earth, Campus de Espinardo, Facultad
17 de Química, 30100 Murcia, Spain.

18 ⁶ Enviroware srl, Concorezzo, MB, Italy.

19 ⁷ Institute of Coastal Research, Chemistry Transport Modelling Group, Helmholtz-Zentrum
20 Geesthacht, Germany.

21 ⁸ INERIS, Institut National de l'Environnement Industriel et des Risques, Parc Alata, 60550 Verneuil-
22 en-Halatte, France.

23 ⁹ Dept. Physical and Chemical Sciences, University of L'Aquila, L'Aquila, Italy.

24 ¹⁰ Center of Excellence CETEMPS, University of L'Aquila, L'Aquila, Italy.

25 ¹¹ Centre for Atmospheric and Instrumentation Research (CAIR), University of Hertfordshire,
26 Hatfield, UK.

27 ¹² European Centre for Medium Range Weather Forecast (ECMWF), Reading, UK.

28 ¹³ Ricardo Energy & Environment, Gemini Building, Fermi Avenue, Harwell, Oxon, OX11 0QR, UK.

29 ¹⁴ Environmental Research Group, Kings' College London, London, UK.

30 ¹⁵ NRC Research Associate at Computational Exposure Division, National Exposure Research
31 Laboratory, Office of Research and Development, United States Environmental Protection Agency,
32 Research Triangle Park, NC, USA

33 ¹⁶ Ramboll Environ, 773 San Marin Drive, Suite 2115, Novato, CA 94998, USA.

34 ¹⁷ Finnish Meteorological Institute, Atmospheric Composition Research Unit, Helsinki, Finland.

35 ¹⁸ Cornell University, Department of Earth and Atmospheric Sciences, Ithaca, USA.

36 ¹⁹ CIEMAT. Avda. Complutense 40., 28040 Madrid, Spain.

37 ²⁰ Computational Exposure Division, National Exposure Research Laboratory, Office of Research and
38 Development, United States Environmental Protection Agency, Research Triangle Park, NC, USA.

39 ^a now at: Section Environmental Meteorology, Division Customer Service, ZAMG e Zentralanstalt für
40 Meteorologie und Geodynamik, 1190 Wien, Austria.

41

42 **Abstract**

43 In the framework of the third phase of the Air Quality Model Evaluation International
44 Initiative (AQMEII3), and as contribution to the second phase of the Hemispheric Transport
45 of Air Pollution (HTAP2) activities for Europe and North America, the impacts of a 20%
46 decrease of global and regional anthropogenic emissions on surface air pollutant levels in
47 2010 are simulated by an international community of regional scale air quality modeling



48 groups, using different state-of-the-art chemistry and transport models (CTM). The emission
49 perturbations at the global level, as well as over the HTAP2-defined regions of Europe, North
50 America and East Asia are first simulated by the global Composition Integrated Forecasting
51 System (C-IFS) model from European Centre for Medium-Range Weather Forecasts
52 (ECMWF), which provides boundary conditions to the various regional CTMs participating
53 in AQMEII3. On top of the perturbed boundary conditions, the regional CTMs used the same
54 set of perturbed emissions within the regional domain for the different perturbation scenarios
55 that introduce a 20% reduction of anthropogenic emissions globally as well as over the
56 HTAP2-defined regions of Europe, North America and East Asia.

57 Results show that the largest impacts over both domains are simulated in response to the
58 global emission perturbation, mainly due to the impact of domestic emissions reductions. The
59 responses of NO₂, SO₂ and PM concentrations to a 20% percent anthropogenic emission
60 reductions are almost linear (~20% decrease) within the global perturbation scenario with
61 however, large differences in the geographical distribution of the effect. NO₂, CO and SO₂
62 levels are strongly affected over the emission hot spots. O₃ levels generally decrease in all
63 scenarios by up to ~1% over Europe, with increases over the hot spot regions, in particular in
64 the Benelux region, by an increase up to ~6% due to the reduced effect of NO_x-titration. O₃
65 daily maximum of 8-hour running average decreases in all scenarios over Europe, by up to
66 ~1%. Over the North American domain, the central-to-eastern part and the western coast of
67 the U.S experience the largest response to emission perturbations. Similar but slightly smaller
68 responses are found when domestic emissions are reduced. The impact of inter-continental
69 transport is relatively small over both domains, however, still noticeable particularly close to
70 the boundaries. The impact is noticeable up to a few percent, for the western parts of the
71 North American domain in response to the emission reductions over East Asia. O₃ daily
72 maximum of 8-hour running average decreases in all scenarios over North Europe by up to
73 ~5%. Much larger reductions are calculated over North America compared to Europe.

74 In addition, values of the Response to Extra-Regional Emission Reductions (RERER) metric
75 have been calculated in order to quantify the differences in the strengths of non-local source
76 contributions to different species among the different models. We found large RERER values
77 for O₃ (~0.8) over both Europe and North America, indicating a large contribution from non-
78 local sources, while for other pollutants including particles, low RERER values reflect a
79 predominant control by local sources.

80 1. Introduction

81 Regional air quality modeling has considerably developed during recent decades, driven by
82 increased concern regarding the impact of air pollution on human health and ecosystems.
83 Numerous air quality models have been developed by research groups worldwide and are
84 being widely used for developing and testing emission control policies. Regional atmospheric
85 chemistry and transport models (CTMs) are widely used to assess the past, present and future
86 levels of air pollutants from continental to regional scales. There are different sources of
87 uncertainties in models such as emissions, meteorology, boundary conditions and chemical
88 schemes that should be taken into account when analyzing results. These uncertainties



89 become more critical when these models are used for regulatory applications such as impacts
90 of emission reductions. Multi-model ensembles can help in reducing this uncertainty and
91 provide a better estimate of impacts under different scenarios (Solazzo et al., 2013; Galmarini
92 et al., 2013; Kioutsooukis et al., 2017).

93 Numerous observational and modeling studies show that long-range transport of pollutants
94 degrade air quality over remote continents (e.g., Wilkening et al., 2000; Holloway et al.,
95 2003; Akimoto, 2003; Fiore et al., 2009). Although the influence of foreign emissions on
96 continental scales is seen most frequently in the free troposphere, surface levels can also be
97 affected, in particular over locations that generally receive clean air masses (e.g. Li et al.,
98 2002). For example, dust storms and biomass burning can influence the tropospheric
99 composition on a hemispheric scale (e.g., Husar et al., 2001; Jaffe et al., 2004). Reducing air
100 pollution levels in surface air would improve public health as exposure to these atmospheric
101 constituents aggravates respiratory illness and leads to premature mortality (World Health
102 Organization, 2013; Im et al., 2017; Liang et al., 2017). However, attributing pollution to
103 specific source regions is complicated due to the different processes influencing
104 intercontinental transport and by a large hemispheric background and the dominance of local
105 emissions in contributing to high levels of particular pollutants, such as ozone (O₃) (e.g. Fiore
106 et al., 2009). Given these difficulties, estimates of source-receptor relationships rely heavily
107 on models.

108 Stjern et al. (2016), using ten models participating in the second Hemispheric Transport of
109 Air Pollution (HTAP2) activity, showed that a 20% reduction of global anthropogenic
110 emissions, leads to significant changes regionally. They found that for North America (NA),
111 black carbon emissions controls in East Asia are more important than domestic mitigation. In
112 the framework of the HTAP2 activity, UN (2007) showed that a 20% reduction of North
113 American NO_x emissions leads to a 0.22 ppb decrease in O₃ levels over Europe (EU), while a
114 20% decrease in East Asian NO_x emissions leads to a decrease of North American surface O₃
115 levels by 0.12 ppb. The impacts of these emissions changes on the O₃ levels in the source
116 regions are much higher. The impact of lateral boundary conditions (LBC) on concentration
117 fields simulated by regional-scale air quality models can also be quite significant (Jimenez et
118 al., 2007; Mathur, 2008; Rudich et al., 2008; Song et al., 2008; Andersson et al., 2015;
119 Giordano et al., 2015; Hogrefe et al., 2017; Solazzo et al., 2017a). Recently, Giordano et al.
120 (2015) showed that the regional models can be very sensitive to the boundary conditions
121 provided by the global models. Tang et al. (2007) showed that the simulated surface levels
122 over polluted areas are usually not as sensitive to the variation of LBCs, but are more
123 sensitive to the magnitude of their background concentrations. Jonson et al. (2017), in the
124 framework of the HTAP2 activity, showed that for ozone the contributions from the rest of
125 the world is larger than the effects from European emissions alone, with the largest
126 contributions from North America and East Asia. The majority of these studies that address
127 impact of emissions on regional and inter-continental transport employ global models on
128 coarse spatial resolution or focus on just a few species, such as O₃ or carbon monoxide (CO).
129 On the other hand, studies using regional chemistry and transport models at finer spatial
130 resolutions mostly focus on sub-regional scales (e.g. Im and Kanakidou, 2012; Huzsar et al.,



131 2016). Therefore, studies addressing multi-pollutant, source-receptor relationships on inter-
132 continental and regional scales can provide valuable information on the impact of domestic
133 and foreign emissions on regional air pollution levels. Multi-model ensembles operating on
134 fine spatial resolutions can increase accuracy and provide an estimate of uncertainty.

135 The Air Quality Model Evaluation International Initiative (AQMEII), coordinated jointly by
136 European Commission, Joint Research Centre (EC-JRC) and the U.S. Environmental
137 Protection Agency (EPA) has brought together regional chemistry and transport modelling
138 groups from Europe and North America since 2008 (Rao et al., 2012; Solazzo et al., 2012a,b;
139 Im et al., 2015 a,b). AQMEII is now running its third phase as a regional sub-project of the
140 larger Hemispheric Transport of Air Pollution (HTAP), which in turn is a taskforce of Long
141 Range Transport of Air Pollution program (LTRAP) of United Nations Economic
142 Commission for Europe (UNECE) (Galmarini et al., 2017). The aim of the study is to assess
143 the impact of global and HTAP2-defined regional anthropogenic emission reductions of 20%
144 in Europe, North America and East Asia on major air pollutant levels over Europe and North
145 America using a multi-model ensemble approach. The study will also investigate the local vs.
146 non-local contributions to different air pollutant levels, adopting the Response to Extra-
147 Regional Emission Reductions (RERER) metric developed by the HTAP2 community
148 (Galmarini et al., 2017).

149 2. Materials and Methods

150 In the framework of the AQMEII3 project, fourteen groups contributed to the simulation of
151 the air pollution levels in Europe (EU) and North America (NA) in the year 2010 (Table 1
152 and Solazzo et al., 2017b). The emission inventories that are used in the second phase of
153 AQMEII for Europe and North America (Im et al., 2015a,b) and extensively described in
154 Pouliot et al. (2015) are also used in AQMEII3. For the EU, the 2009 inventory of MACC
155 anthropogenic emissions was used. In regions not covered by the Monitoring Atmospheric
156 Composition & Climate (MACC) inventory, such as North Africa, five modelling systems
157 have complemented the standard inventory with the HTAPv2.2 datasets (Janssens-Maenhout
158 et al., 2015). For the NA domain, the 2008 National Emissions Inventory was used as the
159 basis for the 2010 emissions with 2010-specific adjustments for major point sources, mobile
160 sources and wildfires (Pouliot et al., 2015). The emissions were then treated with the
161 SMOKE emissions processing system (Mason et al., 2012). For both continents, the regional
162 scale emission inventories were embedded in the global scale inventory (Janssens-Maenhout
163 et al., 2015) to guarantee coherence and harmonization of the information used by the
164 regional and global scale modelling communities (Galmarini et al., 2017). The majority of the
165 European groups used MACC emissions over Europe, while FII and FRES1 supplemented
166 the MACC emissions with HTAP emissions over North Africa (Table 1). For NA, the
167 temporal and vertical allocation of emissions vary between the groups that used the
168 "SMOKE" files (DE1, US1, US3) and the gridded HTAP files (DK1), however the annual
169 total mass are exactly the same. Overall, there was a high level of harmonization of emission
170 inputs even if there were some differences in how they were adapted by each modeling group
171 for their system. Chemical boundary conditions for both domains were provided by the



172 European Center for Medium Range Weather Forecasts (ECMWF) Composition – Integrated
173 Forecast System (C-IFS) model (Flemming et al., 2015)

174 2.1. Emission perturbations

175 The perturbation scenarios feature a reduction of 20% of the anthropogenic emissions
176 globally and in HTAP-defined regions of Europe, North America and East Asia (Table 2).
177 The choice of 20% was motivated by the consideration that the perturbation would be large
178 enough to produce a sizeable impact (i.e. more than numerical noise) even at long distances
179 while small enough to be in the near-linear atmospheric chemistry regime (Galmarini et al.,
180 2017). The emission reductions are implemented in both the global C-IFS model that
181 provides the boundary conditions to the participating regional models, as well as in the
182 regional models. The regional models use the corresponding set of boundary conditions
183 extracted from the C-IFS model. Among the fourteen groups that participated to the
184 AQMEII3 base case simulations, twelve groups from Europe and two groups from North
185 America simulated at least one of the three emission perturbation scenarios, shown in Table
186 1. Two of the European groups (DE1 and DK1) also simulated the base and the three
187 perturbation scenarios for the North American domain.

- 188 - The global perturbation scenario (GLO) reduces the global anthropogenic emissions
189 by 20%. This change has been implemented in the C-IFS global model that provides
190 the boundary conditions to the regional models participating in the AQMEII
191 ensemble. Therefore, the GLO scenario introduces a change in the boundary
192 conditions as well as a 20% decrease in the anthropogenic emissions used by the
193 regional models. Nine groups over the EU domain and four groups over the NA
194 domain have simulated the GLO scenario.
- 195 - The North American perturbation scenario (NAM) reduces the anthropogenic
196 emissions in North America by 20%. This change has been implemented in the C-IFS
197 global model that provides the boundary conditions to the regional models used in the
198 AQMEII ensemble. Therefore, the NAM scenario introduces a change in the
199 boundary conditions while anthropogenic emissions remain unchanged for Europe,
200 showing the impact of long-range transport of North American pollutants to Europe
201 while for North America, the scenario introduces a 20% reduction of anthropogenic
202 emissions in the HTAP-defined North American region, showing the contribution
203 from the domestic anthropogenic emissions. Seven groups over the EU domain and
204 three groups over the NA domain have simulated the NAM scenario.
- 205 - The European perturbation scenario (EUR) reduces the anthropogenic emissions in
206 the HTAP-defined Europe domain by 20%. The EUR scenario introduces a change in
207 the anthropogenic emissions over the EUR region in the CTMs, showing the
208 contribution from the domestic anthropogenic emissions. Six groups have simulated
209 the EUR scenario over the EU domain.
- 210 - The East Asian perturbation scenario (EAS) reduces the anthropogenic emissions in
211 East Asia by 20%. Similar to the NAM scenario for the EU domain, the EAS scenario
212 introduces a change in the boundary conditions while anthropogenic emissions remain
213 unchanged in the regional models, showing the impact of long-range transport from



214 East Asia on the NA concentrations. Four groups have simulated the EAS scenario
215 over the NA domain.

216 In AQMEII, all participating groups were required to upload modelled hourly surface
217 concentrations to the ENSEMBLE system at EC-JRC, at specified monitoring stations in EU
218 and NA, as well as surface gridded data (Galmarini et al, 2012; Im et al., 2015a, b; Solazzo et
219 al., 2017b). This study investigates the impacts of emission perturbations and boundary
220 conditions on O₃, NO₂, CO, SO₂, PM₁₀ and PM_{2.5} levels over Europe and North America.

221 Differences between each perturbation scenario and the base case (C-IFS global and regional
222 models run with baseline emissions) are calculated from the gridded hourly pollutant fields,
223 which are then monthly and annually averaged in order to estimate the impact of the
224 perturbation of the corresponding emission or boundary condition.

225 To estimate the contribution of foreign emission perturbations relative to the GLO
226 perturbation, we have also calculated the RERER metric (Galmarini et al., 2017; Huang et al.,
227 2017; Jason et al., 2017). For Europe, RERER is calculated using the differences between the
228 GLO vs BASE as well as the differences between EUR vs. BASE simulations for Europe
229 (Eq. 1) while for North America; RERER is calculated using the differences between the
230 GLO vs BASE and NAM vs. BASE simulations (Eq. 2).

$$231 \quad RERER_{EUR} = \frac{R_{GLO} - R_{EUR}}{R_{GLO}} \quad \text{Eq. 1}$$

$$232 \quad RERER_{NAM} = \frac{R_{GLO} - R_{NAM}}{R_{GLO}} \quad \text{Eq. 2}$$

233 where R_{GLO} is the response of the concentration of a given species to global emission
234 reduction, R_{EUR} is the response of a concentration of a species to the EUR perturbation for the
235 European domain, and R_{NAM} is the response of a concentration of a specie to the NAM
236 perturbation for the North American domain. Therefore, a subset of modelling groups that
237 have conducted the three simulations (BASE, GLO and EUR/NAM for Europe and North
238 America, respectively) have been used in the metric calculations (see Table 1). The higher the
239 local response is, the smaller the RERER metric is. The RERER value can exceed the value 1
240 when emission reductions lead to increasing concentrations (e.g., O₃ titration by nitrogen
241 monoxide, NO).

242 3. Results

243 3.1. Model Evaluation

244 The base case simulation of each model has been evaluated on a monthly basis using
245 available surface observations from Europe and North America. The observational data used
246 in this study are the same as the dataset used in the second phase of AQMEII (Im et al.,
247 2015a,b). The data were provided from the surface air quality monitoring stations operating
248 in EU and NA. In EU, surface data were provided by the European Monitoring and
249 Evaluation Programme (EMEP, 2003; <http://www.emep.int/>) and the European Air Quality
250 Database (AirBase; <http://acm.eionet.europa.eu/databases/airbase/>). NA observational data



251 were obtained from the NAtChem (Canadian National Atmospheric Chemistry) database and
252 from the Analysis Facility operated by Environment Canada (<http://www.ec.gc.ca/natchem/>).

253 The model evaluation results for each model are presented in Fig. 1 and 2, and in Table 3,
254 along with the results for the multi model (MM) mean and median values. The results show
255 that the monthly variations of gaseous pollutants are well captured by all models with
256 correlation coefficients (r) generally higher than 0.70. The biases in simulated O₃ levels are
257 generally less than 10% with a few exceptions of up to -35%. The temporal variations of NO₂
258 levels are also well simulated ($r > 0.7$), but exhibit much higher biases, with underestimations
259 up to 75%. CO levels are underestimated by up to 45% while a majority of the models
260 underestimated SO₂ levels by up to 68%. Few models overestimated SO₂ by up to 49%. PM₁₀
261 and PM_{2.5} levels are underestimated by 20% to 70%. Slightly higher biases are calculated for
262 the PM₁₀ levels. A more comprehensive evaluation of the models is presented in Solazzo et
263 al. (2017b), Galmarini et al. (2017) and Im et al. (2017).

264 C-IFS base case results have also been evaluated along with the regional CTMs, as presented
265 in Fig. 1 and 2 and in Table 3. The seasonal variations for O₃, NO₂, CO and SO₂ are well
266 captured with high correlation values of ~ 0.9 . PM₁₀ and PM_{2.5} showed a different seasonal
267 cycle than the observation by not reproducing the wintertime maxima ($r \sim -0.7$). C-IFS model
268 underestimates O₃ and CO by $\sim 20\%$ over Europe while NO₂ is slightly overestimated
269 ($NMB = 7\%$). SO₂ is overestimated by $\sim 10\%$ over Europe, while PM₁₀ and PM_{2.5} levels are
270 largely underestimated by $\sim 60\%$, which can be attributed to the lack of secondary aerosol
271 mechanism in the bulk C-IFS model. Over the North American domain, C-IFS well captures
272 the seasonal variations of O₃, NO₂ and CO with correlation coefficients larger than 0.7, while
273 the seasonal variation of SO₂ is not captured by the model ($r = 0.04$). The seasonal variations
274 of PM₁₀ and PM_{2.5} are also poorly captured ($r < 0.2$). North American O₃ levels are slightly
275 underestimated ($NMB = -10\%$), while NO₂ and CO are overestimated by $\sim 40\%$ and 20% ,
276 respectively. SO₂ is overestimated by 35% while PM₁₀ is largely underestimated by $\sim 80\%$
277 and PM_{2.5} by $\sim 40\%$. Over both Europe and North America, the wintertime PM levels are
278 underestimated due to lack of secondary aerosols while the spring summer peaks are
279 attributed to long range transport of desert dust from the Sahara, which effect mainly the
280 South East of North America.

281 3.2. Perturbation Analyses

282 The annual mean relative differences of each perturbation scenario from the base case
283 scenario, averaged over all stations, are provided in Table 4 (EU) and Table 5 (NA) for each
284 modeling group, along with the results for the MM ensemble mean and median. The base
285 case monthly mean time series for the participating groups are provided in Fig.1 and Fig. 2
286 for each pollutant, while Fig.3 and Fig. 4 shows the annual mean spatial distribution of the
287 pollutants from the MM ensemble mean calculations over Europe and North America,
288 respectively. As seen in the time series figures, there is a large spread among different
289 groups, owing to the different models used and the different sets of anthropogenic emissions
290 (Table 1). However, the temporal variation is consistent among all models, in particular for
291 the gaseous species.



292 3.2.1. Impact of the global emission reduction scenario (GLO)

293 3.2.1.1. Europe

294 The monthly time series of the differences between the GLO and the BASE simulations for
295 each pollutant are presented in Fig. 5. The annual differences are reported in Table 4.
296 Regarding the primary gaseous pollutants, all models simulate the smallest differences during
297 the summer months while the differences are largest in winter. For O₃, the simulated
298 differences are positive in winter and negative in summer for all models except for DE1 that
299 simulated a decrease in all months. Results suggest that wintertime O₃ over Europe is mainly
300 controlled by anthropogenic emissions. For the other pollutants, results suggest that their
301 levels are mainly controlled by anthropogenic emission throughout the year. The annual
302 difference is smallest for O₃, with a reduction of -0.34 ± 1.23 ppb ($-1.04 \pm 4.00\%$). The annual
303 mean value of the O₃ daily maximum of 8-hour running average decreases by -0.53 ± 1.50 ppb
304 ($-1.62 \pm 3.99\%$). NO₂ levels decreased by 0.97 ± 0.45 ppb ($19.34 \pm 1.59\%$) over Europe while
305 CO levels decreased by 17.35 ± 4.03 ppb ($11.22 \pm 1.17\%$), SO₂ levels by 0.18 ± 0.05 ppb
306 ($20.87 \pm 0.93\%$), PM₁₀ by 2.38 ± 0.68 μgm^{-3} ($15.84 \pm 2.12\%$) and PM_{2.5} by 2.02 ± 0.52 μgm^{-3}
307 ($18.30 \pm 1.75\%$). Vivanco et al. (2017) found similar reductions regarding the deposition of
308 sulfur and nitrogen species over Europe. Almost all models simulate an overall decrease of
309 annual mean O₃ levels over EU (-0.94% to -4.65%), with the exception of TR1 that simulated
310 an increase of 9.31%. Regarding other pollutants, all models simulate a decrease during the
311 simulation period. In general, DE1 and TR1 model groups stand out for introducing the
312 smallest and largest differences, particularly for O₃, NO₂, and PM.

313 The geographical distribution of the change in annual mean concentrations in the GLO
314 scenario as simulated by the MM mean is presented in Fig. 6. Regarding O₃, most of Europe
315 is characterized by decreased concentrations (Fig.6a). Over central Europe, where most of the
316 primary emissions are located (e.g. NO_x), O₃ levels slightly increase by ~2%. Emission
317 hotspots, in particular the Benelux area stands out with largest increases (~6%) due to
318 decreased NO_x-titration effect, which can also be seen in Fig. 6b. In addition, O₃ levels over
319 the northern parts of Germany and France, and southern UK are increasing in response to
320 emission reductions. There is also a clear decrease in CO levels (Fig.6c), in particular over
321 central Europe by up to ~16%. All primary species decrease over the whole domain,
322 especially over the industrial hot spots such as in Poland, Po Valley and the Benelux area
323 (Fig.6d). PM levels decrease throughout the domain by up to ~20% (Fig.6e and f).

324 3.2.1.2. North America

325 The seasonal variation of the impact of 20%-decreased global emissions on the North
326 American pollutant levels are presented in Fig.7. All models simulated a small decrease of
327 3% to 5% (Table 5) in O₃ levels with the largest differences in spring to summer (Fig.7a).
328 The mean response to the emission perturbation is estimated to be -1.39 ± 0.27 ppb ($-3.52 \pm$
329 0.80%). The annual mean value of the O₃ daily maximum of 8-hour running average
330 decreases by -1.93 ± 0.14 ppb ($-4.51 \pm 0.45\%$). All models simulated a largest NO₂ response in
331 winter. Most models simulated a decrease of NO₂ levels while DK1 estimated an increase



332 (Fig.7b). As shown in Table 5, the models simulated a NO₂ response of ~0.4 – 1.2 ppb (-17.8
333 ± 0.78%). Regarding CO, all models simulated very clear seasonal profile of the response to
334 emission reductions, with maximum change in late winter/early spring and the minimum
335 change in summer. Most models simulated a change around -15 to -25 ppb (~11%); with the
336 exception of the DE1 model simulating a decrease of ~9 ppb (~7.9%). The MM mean
337 response is calculated to be 19.2 ± 6.9 ppb (-11 ± 2.3%). The impact of the emission
338 reduction on SO₂ levels was calculated to be -0.25 ppb to -0.48 ppb (-20.3 ± 0.2%).

339 The response of PM₁₀ levels to the global emission reduction was calculated to be -2.4 ± 1.8
340 μg m⁻³ (-32.1 ± 26.6%) (Table 5). The largest relative change was calculated for DE1 (~63%).
341 DK1 has almost a flat response around -1 μg m⁻³, while DE1, which is overlapped with the
342 Median line, and US3 have maximum responses in early spring and mid-autumn, while they
343 simulate a minimum response in winter and late spring. Regarding PM_{2.5}, the multi-model
344 mean response was calculated to be -1.5 ± 0.9 μg m⁻³ (-17.2 ± 1.8%). DK1 (overlapped with
345 the Median) and US3 simulated the minimum response in May (Fig.7f), while US3 has a
346 slightly higher second minimum in September. This minimum is also simulated by DE1 as
347 the minimum response. DE1 simulates the lowest response among the three models.

348 The spatial distributions of response of different pollutants to the GLO scenario are presented
349 in Fig.8. O₃ levels are reduced over most of the domain (Fig.8a), with slight increases over
350 the emission hotspots due to reduced effect of NO_x-titration, as seen in Fig.8b, as well as
351 decreased CO levels over the whole domain (Fig.8c). SO₂ levels are also decreased
352 throughout the domain (Fig.8d), with the largest reductions over the Atlantic (attributable to
353 reduction in shipping emissions). The western part of the continent is characterized by the
354 lowest reductions. PM levels are reduced throughout the domain by up to 25% (Fig.8e and f),
355 with the largest reductions over the eastern and central parts of the domain. A large decrease,
356 more pronounced in the PM_{2.5} response, can also be seen over California in the western
357 coastal United States.

358 3.2.2. Impact of the North American emission reduction scenario (NAM)

359 3.2.2.1. Europe

360 NA emission reductions account for a reduction of European O₃ levels of -0.22±0.07 ppb (-
361 0.75±0.14%), with all models simulating a decrease of -0.51% to 0.86%, except for the ES1
362 model that simulated an increase of 1.31% (Table 4). This decrease is in agreement with
363 previous studies, such as the HTAP2 study (UN, 2017) that calculated an O₃ reduction over
364 Europe of 0.22 ppb in response to a 20% decrease in the North American NO_x emissions, and
365 Fiore et al. (2009) that simulated a MM mean response of -0.4 ppb in response to a 20%
366 reduction of anthropogenic emissions in North America. NO₂ levels increase slightly by
367 0.16±0.01%. The annual mean value of the O₃ daily maximum of 8-hour running average
368 decreases by -0.15±0.27 ppb (-0.45±0.77%). CO levels also decreased over the EU domain
369 by -1.39±0.27 ppb (-0.96±0.22%), much higher than ~0.1 ppb calculated by Fiore et al.
370 (2009). PM₁₀ and PM_{2.5} levels also decreased slightly by -0.03±0.03 μg m⁻³ (-0.21±0.7%) and
371 -0.02±0.02 μg m⁻³ (-0.18±0.25%), respectively. The models had different SO₂ responses to



372 the NA emissions. Overall, DE1, ES1 and FRES1 simulated almost no change in the surface
373 SO₂ levels while DK1, ES1 and TR1 simulated an increase (0.10%, 5.75% and 0.01%,
374 respectively) and FII and UK1 simulated a decrease (-0.02% and -0.03%, respectively).
375 Different responses can be due to different model setups including aqueous chemistry,
376 vertical resolutions and aerosol modules (Solazzo et al., 2017).

377 All models were consistent in simulating the largest impact on O₃ during spring and a second
378 lower peak in autumn (Fig.9a). Surface mean NO₂ concentrations (Fig.9b) increased in most
379 models except for FRES1 that simulated a small decrease except for winter. FII also
380 simulated a decrease during the winter period extending to the transition periods. All models,
381 except for ES1, simulated a similar response of CO concentrations to perturbation to NA
382 emissions, with a distinct seasonality (Fig.9c). The SO₂ response in models is also consistent
383 except for the winter period where there is a large spread in magnitude and the sign of the
384 response (Fig.9d).

385 O₃ levels decreased slightly over the entire European domain by up to 3% (Fig.10a). The
386 largest impact is simulated over the western boundary and gradually decreases eastwards.
387 The response of O₃ levels to NAM emissions is more evident during spring where there is a
388 clear transport from Atlantic to the western/northwestern parts of Europe such as the U.K,
389 northern France and Scandinavia (Fig. S2a). The transport of Atlantic air masses is also
390 shown for the springtime CO levels over Europe (Fig. S2a). The ensemble mean simulates a
391 slight increase of up to 3% in NO₂ levels over Europe (Fig.10b). Along with the O₃ levels,
392 CO levels show the largest decrease over northwestern Europe by up to ~2%. SO₂ levels
393 increased over the whole domain, in particular over Eastern Europe and the Alpine region
394 (Fig.10d), due to a decrease in the oxidative capacity of the atmosphere (see Fig.10a for O₃),
395 leading to a decrease in the SO₂ to SO₄ conversion. This results in an increase of the SO₂
396 levels and a decrease in the PM_{2.5} levels (Fig.10e and f).

397 3.2.2.2. North America

398 The response of North American pollutant levels to a 20% reduction of North American
399 anthropogenic emissions (implemented in both C-IFS and the regional CTMs) are presented
400 in Table 5. The NAM scenario led to a decrease of annual mean O₃ levels over North
401 America by -0.36 ppb (US3) to -0.92 ppb (DE1), with *MM* ensemble mean calculated to be -
402 0.65±0.28 ppb (-1.45±0.88%), in agreement with Fiore et al. (2009) that calculated a decrease
403 of ~1 ppb. The annual mean value of the O₃ daily maximum of 8-hour running average
404 decreases by -1.11±0.11 ppb (-2.60±0.36%), very similar to the change over Europe.
405 Consequently, the largest change in NO₂ levels were simulated by US3 (-1.17 ppb) and
406 smallest by DE1 (-0.36 ppb). The *MM* mean response of NO₂ is calculated to be -0.71±0.41
407 ppb (-17.24±0.58%). Similar to NO₂, the largest response in CO levels were simulated by
408 US3 (-19.87 ppb) and the smallest by DE1 (-3.84 ppb), leading to a *MM* mean response of -
409 12.35±8.06 ppb (-7.01±3.60%). As seen in Table 5, DE1 simulated a much lower absolute
410 and relative change in CO response compared to DK1 and US3. SO₂ levels decreased by -
411 0.32 ppb to -0.48 ppb, leading to a *MM* mean response of -0.37±0.09 ppb (-20±0.12%). PM₁₀
412 levels decreased -1.78±2.08 µgm⁻³ (-15.78±3.26%). As seen in Table 5, DK1, simulated a



413 very low response to the NAM scenario, by $\sim 0.60 \mu\text{g m}^{-3}$, compared to the DE1 and the US3
414 groups that simulated a PM_{10} response of $-2.02 \mu\text{g m}^{-3}$ and $-4.19 \mu\text{g m}^{-3}$, respectively.
415 However, the relative responses are not very different between the different groups ($\sim 16\%$).

416 The response of O_3 to the NAM scenario is largest in summer (Fig.11a): June for DK1 and
417 US3 and August for DE1. The O_3 response clearly shows a difference from the GLO
418 response in spring, suggesting the impact of long-range transport in spring that does not
419 appear in the perturbation of the local emissions only. The largest NO_2 response (Fig.11b) is
420 simulated by US3, similar to the response to the GLO scenario. The response of CO to the
421 reductions in local emissions (Fig.11c) is different from the response to the global reduction,
422 where DK1 and US3 has the minimum response in spring and DE1 has the minimum
423 response in autumn. The response of SO_2 and PM to GLO and NAM are similar, suggesting
424 the main drivers of SO_2 and PM levels are local emissions.

425 Annual mean O_3 levels show large reductions ($\sim 20\%$) over the eastern parts of the domain,
426 while there are slight increases or less pronounced decreases over the western parts of the
427 domain (Fig.12a), associated with larger NO_x reductions (Fig.12b). CO and SO_2 levels are
428 mostly reduced over the central to eastern parts of the domain (Fig.12c and d, respectively),
429 with shipping impacts over the Atlantic being more pronounced on SO_2 levels. The western
430 parts of the U.S. experiences smaller SO_2 reductions ($\sim 5\text{-}10\%$) and slight increases over the
431 southwestern U.S. The response of PM to the NAM scenario (Fig.12e and f) is very similar to
432 the response to the GLO scenario (Fig.8e and f).

433 3.2.3. Impact of the European emission reduction scenario (EUR)

434 O_3 levels increase slightly by 0.01 ± 0.40 ppb ($0.25 \pm 1.35\%$) in response to the 20% reduction
435 of the anthropogenic emissions from Europe (Table 4). This response is much lower than
436 Fiore et al. (2009) that calculated a MM mean response of 0.8 ppb. However, as seen in
437 Fig.13a, the positive mean response together with the large standard deviation is due to the
438 DE1 model that simulated a decrease (-2.33%), while other groups simulated an increase
439 (0.39% to 1.72%). There is a distinct seasonality in the response with winter levels increasing
440 with reduced emissions and summer levels decreasing, following the emission temporal
441 variability. The annual mean value of the O_3 daily maximum of 8-hour running average
442 decreases by -0.21 ± 0.10 ppb ($-0.62 \pm 0.24\%$). NO_2 concentrations decreased by -0.75 ± 0.26
443 ($17.68 \pm 0.90\%$), with a similar seasonal response of SO_2 levels ($-17.52 \pm 1.70\%$) and CO levels
444 ($-6.26 \pm 1.07\%$), consistent with the findings of Vivanco et al. (2017). An opposite seasonal
445 variation is calculated for the O_3 response (Fig. 13.b-d)., The DE1 model also stands out in
446 the NO_2 response together with the FRES1 model in the magnitude of the response (Fig.13b).
447 PM_{10} and $\text{PM}_{2.5}$ levels have similar responses to the emissions reduction ($-14.43 \pm 2.84\%$ and
448 $-15.67 \pm 2.12\%$, respectively) with similar seasonality.

449 The MM mean geographical distribution of the O_3 response is very similar with that of the
450 GLO perturbation (Fig.14a), with relatively smaller decreases by up to $\sim 3\%$. O_3 levels
451 increase over the central and in particular over northwestern Europe by up to $\sim 6\%$. NO_2
452 levels decrease uniformly over the entire domain by up to $\sim 20\%$ (Fig.14b). CO levels



453 decrease over the emission sources, mainly over central and Eastern Europe (Fig.14c). PM
454 levels also decrease over the entire domain, especially over central and Eastern Europe
455 (Fig.14e and f).

456 3.2.4. Impact of the East Asian emission reduction scenario (EAS)

457 As seen in Table 5, the impacts of East Asian emissions on North American O₃ levels are
458 much lower than the impacts from the reductions in global and local emissions. The largest
459 impact is simulated by DE1 as -0.99 ppb (-0.35%), while other models give similar responses
460 (~0.60 ppb; -0.20%). The O₃ response as calculated by the MM mean ensemble is -0.25±0.07
461 ppb, in agreement with the HTAP2 findings and Fiore et al. (2009). The annual mean value
462 of the O₃ daily maximum of 8-hour running average decreases by -0.28±0.07 ppb (-
463 0.65±0.20%). NO₂ and SO₂ response to reductions in EAS emissions were simulated to be
464 very small (-0.04±0.08% and 0.01±0.02%, respectively). The CO response to EAS was
465 simulated to be -2.60 ppb (DE1) to -4.16 ppb (DK1), with the MM mean response of -
466 3.37±0.68 ppb (-2±0.29%). Regarding PM₁₀, DE1 simulated a very large response (~-0.56
467 μgm⁻³) compared to DK1 and US3 (~-0.05 μgm⁻³), leading to a MM mean response of -
468 0.21±0.30 μgm⁻³ (-5.63±8.50%). However, the PM_{2.5} response was much lower (-0.02±0.03
469 μgm⁻³; -0.20±0.35%), suggesting that the PM_{2.5} levels are largely driven by local emissions.

470 The O₃ response to EAS emission reductions was highest in spring and autumn, suggesting
471 that long-range transport is important in these seasons (Fig.15a). The NO₂ response was
472 negative, being maximum in winter and minimum in summer, except for DK1 showing an
473 increase in NO₂ levels in all seasons (Fig.15b). The impact of EAS emissions on North
474 American CO levels showed a distinct seasonality (Fig.15c), similar to the impact of the
475 global emission reductions (Fig.5c), suggesting that regional CO levels over North America
476 are driven by both local emissions and long-range transport. The response of SO₂ to East
477 Asian emission reductions varied largely from model to model with US3 showing an overall
478 reduction while DE1 and DK1 simulated increases in winter, spring, and autumn, and
479 decreases in summer (Fig.15d). The PM₁₀ response simulated by DK1 (overlapped with the
480 median) and US3 were simulated to be small, being largest in spring (Fig.15e). However,
481 DE1 simulated a large and opposite response, with spring having the smallest response and
482 winter with the largest response. DE1 also simulated a different PM_{2.5} response in terms of
483 the sign of the change and thus, seasonality in response to DK1 and US3 (Fig.15f). Largest
484 differences were simulated in spring, similar to PM₁₀ by DK1 and US3, while DE1 simulated
485 the largest response in winter and summer and the spring response was minimum.

486 The impact of the East Asian emissions over the western parts of North America is clearly
487 seen for all pollutants in Fig.16. The impacts are low for all pollutants, being up to 5%. The
488 impacts are particularly pronounced for CO (Fig.16c), SO₂ (Fig.16d) and PM (Fig.16e and f).
489 The largest O₃ response was simulated over the northwestern parts of North America
490 (Fig.16a). The springtime transport of O₃ from East Asia is more evident compared to the
491 annual average of the perturbation response (Fig. S3a), where the western NA O₃ levels
492 decrease by up to ~1.5%. The springtime CO levels also decrease by up to 6% (Fig. S3b),
493 showing the importance of long-range transport from East Asia.



494 3.2.5. RERER analyses

495 As discussed in Section 2, the RERER metric (Galmarini et al., 2017; Hang et al., 2017;
496 Jason et al., 2017) is designed to quantify the relative impact of local vs. non-local emission
497 sources on pollutant levels in the receptor regions EU and NA. Using gridded hourly
498 pollutant concentrations from the base case, GLO and EUR simulations, the RERER metrics
499 for the EU have been calculated for the annual mean concentrations response for the
500 individual groups as well as for the ensemble mean. For the NA domain. The RERER metrics
501 have been calculated using the base case, GLO and NAM simulations. Table 6 presents the
502 RERER metric calculated for the European domain. The table shows differences in the
503 strengths of non-local source contributions to different species among the different models.
504 Regarding the RERER metric for O₃ in Europe, most values calculated are below one, except
505 for the IT1 model, which shows a significant increase of O₃ levels in Europe in response to
506 emission reductions compared with the other models. A RERER value of 0.8-0.9 is calculated
507 for the majority of models, implying the dominance of non-local sources in Europe, except
508 for the DE1 model, where the RERER value is lower (~0.5), giving an equal contribution of
509 local vs. non-local sources in Europe. The MM mean RERER value for O₃ is ~0.8, showing a
510 much larger contribution of non-local sources compared to local sources in Europe. This
511 result is in agreement with, however slightly smaller, Jonson et al. (2017) that calculated a
512 MM mean RERER value of 0.89.

513 Regarding NO₂, the RERER metrics (< 0.4) show that NO₂ is controlled by local sources. In
514 addition, the RERER metrics calculated for DE1 and FI1 are slightly negative, implying that
515 the signal is not sensitive to non-local emissions. RERER calculated for the ensemble mean
516 for NO₂ (~0.2) also shows the high sensitivity of NO₂ concentrations to local sources. The
517 RERER metric calculations for CO shows similar contributions from local vs. non-local
518 sources, with RERER values of 0.4-0.6, except for IT1. IT1 has a RERER metric value of
519 ~0.9 suggesting a large contribution of non-local sources, leading to the higher sensitivity of
520 CO to non-local sources compared to other model groups. The RERER values calculated for
521 the ensemble mean (~0.6) shows a slightly larger contribution of non-local sources compared
522 to local sources. The MM mean RERER value of 0.55 for CO from this study is in very good
523 agreement with Jonson et al. (2017) that calculated a MM mean RERER of 0.51. RERER
524 metrics calculated for SO₂ are also in the low range (0-0.4). While DE1 and FI1 show almost
525 no signal for the non-local contribution, DK1, IT1 and UK1 are in the higher end of the
526 range. The CO MM mean RERER value of ~0.3 shows that CO levels are largely controlled
527 by local emissions. Finally, the metrics calculated for PM₁₀ and PM_{2.5} shows that local
528 sources are the main contributor to the PM levels in Europe (RERER = ~0 - 0.3), leading to
529 an ensemble mean contribution of local sources (RERER = ~0.2).

530 Regarding the local vs. non-local contributions to different pollutants over the North
531 American domain, three groups out of four simulated the GLO and NAM scenarios needed to
532 calculate the RERER metrics. RERER metrics show that O₃ is largely controlled by non-local
533 sources. European model groups DE1 and DK1 simulate a larger influence of non-local
534 sources (~0.8 - ~0.9) compared to the US3 group, which simulated lower RERER metric
535 values of ~0.5, indicating that O₃ levels are driven equally by local and non-local sources.



536 This lower value is also consistent with the findings of Huang et al. (2017), who simulated
537 the largest impacts on O₃ in May and June with RERER values around ~0.5. The ensemble
538 mean shows that O₃ responses are largely attributable to non-local sources (RERER = ~0.8),
539 which are similar to those found for Europe. RERER metric values calculated for NO₂ by
540 different models (RERER = ~0 – ~0.2) and the ensemble mean (RERER = 0.05) clearly
541 shows that NO₂ is controlled by local sources, similar to the Europe case. The sensitivity of
542 CO to local and non-local sources are similar to those for O₃, with DE1 and DK1 simulating a
543 large contribution from non-local sources while US1 shows that CO is controlled equally by
544 local and non-local sources (RERER = 0.5). Similar to NO₂, all models show that SO₂ is
545 largely driven by local sources with RERER values between ~0.1 and ~0.2. Regarding the
546 particles, models simulate very similar responses to changes in the local and non-local
547 sources. RERER values are calculated to be ~0.08 and ~0.11 for PM₁₀ and PM_{2.5},
548 respectively, showing the large local contribution compared to non-local sources.

549

550 CONCLUSIONS

551 In the framework of the third phase of the Air Quality Model Evaluation International
552 Initiative (AQMEI3), the impacts of local vs. foreign emissions over the European and North
553 American receptor regions are simulated by introducing a 20% decrease of global and
554 regional emissions by research groups, using different state-of-the-art chemistry and transport
555 models. The emission perturbations were introduced globally, as well as over the HTAP2-
556 defined regions of Europe, North America and East Asia. Base case and the perturbation
557 scenarios are first simulated using the global C-IFS global model, which provides the
558 boundary conditions to the regional CTMs.

559 The base case simulation of each model has been evaluated against surface observations from
560 Europe and North America. The temporal variabilities of all pollutants are well captured by
561 all models with correlations generally higher than 0.70. O₃ levels are generally simulated
562 with a *MNB* less than 10% with few exceptions of *MNB* values up to -35%. NO₂, CO and
563 SO₂ levels are simulated with underestimations up to 75%, 45% and 68%, respectively. PM₁₀
564 and PM_{2.5} levels are underestimated by 20% to 70%, with slightly higher biases in PM₁₀
565 levels.

566 Results from the perturbation simulations show that the largest impacts over both Europe and
567 North American domains are simulated in response to the global emission perturbation
568 (GLO). These responses are similar, however slightly lower, as compared to the local
569 emission perturbation scenarios for Europe (EUR) and North America (NAM). In contrast to
570 the GLO scenario, O₃ levels over Europe slightly increase by 0.13 ppb (0.02%). The annual
571 mean value of the O₃ daily maximum of 8-hour running average decreases in all scenarios
572 over Europe, highest in the GLO scenario by ~1% and lowest in the NAM scenario by
573 ~0.3%. Over North America, the annual mean value of the O₃ daily maximum of 8-hour
574 running average decreased by ~5% in the GLO scenario, 3% in the NAM scenario and 0.7%
575 in the EAS scenario. The impact of foreign emissions simulated by the NAM scenario for



576 Europe and EAS scenario for North America were found to be lowest, however still
577 noticeable, particularly close to the boundaries. This impact is especially noticeable (up to
578 only a few percent) for the western parts of the North American domain in response to the
579 emission reductions over East Asia. The response is almost linear (~20% decrease) to the
580 change in emissions for NO₂, SO₂ and PM in the global perturbation scenario (GLO), while
581 O₃ levels decrease slightly (~1%).

582 Despite these small differences, there are large geographical differences. NO₂, CO and SO₂
583 levels are mainly affected over emission hot spots in the GLO scenario as well as in the EUR
584 scenario for Europe and the NAM scenario for North America. O₃ levels increase over the hot
585 spot regions, in particular the Benelux region in Europe, by up to ~6% due to the reduced
586 effect of NO_x-titration. Over the North American domain, the central-to-eastern part and the
587 western coast of the U.S experience the largest response to the global emission perturbation.
588 For most of the pollutants, there is distinct seasonality in the responses particularly to the
589 global and local emission perturbations. The largest responses are calculated during winter
590 months, where anthropogenic emission are highest, except for O₃, where largest responses are
591 seen during spring/summer months, suggesting photochemistry still plays an important role in
592 O₃ levels.

593 The RERER metrics have been calculated to examine the differences in the strengths of non-
594 local source contributions to different species among the different models. The large RERER
595 values over Europe and North America for O₃ (~0.8), show a larger contribution of non-local
596 sources, while for other gaseous pollutants (NO₂, CO and SO₂) and particles (PM₁₀ and
597 PM_{2.5}), low RERER values (< 0.5) indicate that these pollutants are largely controlled by
598 local sources. Results show that the contribution of local sources on NO₂, SO₂ and PM levels
599 are larger in North America compared to Europe, while for CO, local sources have a larger
600 share in Europe in comparison with North America.

601 Overall results show that there is a large spread among the models, although the majority of
602 the models simulate a similar seasonal variation. These differences suggest that despite the
603 harmonization of inputs, such as emissions and boundary conditions, to regional models,
604 there are still large differences between models, such as different gas phase and aerosol
605 modules, deposition schemes, meteorological drivers and spatial and vertical resolutions.
606 Therefore, the use of multi model ensembles can help to reduce the uncertainties inherent in
607 individual models.

608

609 ACKNOWLEDGEMENTS

610 We gratefully acknowledge the contribution of various groups to the third air Quality Model
611 Evaluation international Initiative (AQMEII) activity. Joint Research Center Ispra/Institute
612 for Environment and Sustainability provided its ENSEMBLE system for model output
613 harmonization and analyses and evaluation. The views expressed in this article are those of
614 the authors and do not necessarily represent the views or policies of the U.S. Environmental
615 Protection Agency. Aarhus University gratefully acknowledges the NordicWelfAir project



616 funded by the NordForsk's Nordic Programme on Health and Welfare (grant agreement no.
617 75007), the REEEM project funded by the H2020-LCE Research and Innovation Action
618 (grant agreement no.: 691739), and the Danish Centre for Environment and Energy (AU-
619 DCE). University of L'Aquila thanks the EuroMediterranean Center for Climate Research
620 (CMCC) for providing the computational resources. RSE contribution to this work has been
621 financed by the research fund for the Italian Electrical System under the contract agreement
622 between RSE S.p.A. and the Ministry of Economic Development – General Directorate for
623 Nuclear Energy, Renewable Energy and Energy Efficiency in compliance with the decree of
624 8 March 2006. CIEMAT has been financed by the Spanish Ministry of Agriculture and Food,
625 Fishing and Environment. University of Murcia thanks the Spanish Ministry of Economy for
626 the research contract CGL2014-59677-R (also partially funded by the FEDER programme).

627

628 **REFERENCES**

629 Akimoto, H. (2003), Global air quality and pollution, *Science*, 302, 1716–1719,
630 doi:10.1126/science.1092666.

631 Andersson, E., Kahnert, M., and Devasthale, A.: Methodology for evaluating lateral
632 boundary conditions in the regional chemical transport model MATCH (v5.5.0) using
633 combined satellite and ground-based observations, *Geosci. Model Dev.*, 8, 3747-3763,
634 <https://doi.org/10.5194/gmd-8-3747-2015>, 2015.

635 Fiore, A., Dentener, F., Wild, O., Cuvelier, C., Schultz, M., Textor, C., Schulz, M., Atherton,
636 C., Bergmann, D., Bey, I., Carmichael, G., Doherty, R., Duncan, B., Faluvegi, G., Folberth,
637 G., Garcia Vivanco, M., Gauss, M., Gong, S., Hauglustaine, D., Hess, P., Holloway, T.,
638 Horowitz, L., Isaksen, I., Jacob, D., Jonson, J., Kaminski, J., Keating, T., Lupu,
639 A., MacKenzie, I., Marmer, E., Montanaro, V., Park, R., Pringle, K., Pyle, J., Sanderson, M.,
640 Schroeder, S., Shindell, D., Stevenson, D., Szopa, S., Van Dingenen, R., Wind, P., Wojcik,
641 G., Wu, S., Zeng, G., and Zuber, A.: Multi-model estimates of intercontinental source-
642 receptor relationships for ozone pollution, *J. Geophys. Res.*, 114,
643 doi:10.1029/2008JD010816, 2009.

644 Flemming, J., Huijnen, V., Arteta, J., Bechtold, P., Beljaars, A., Blechschmidt, A.-M.,
645 Diamantakis, M., Engelen, R. J., Gaudel, A., Inness, A., Jones, L., Josse, B., Katragkou, E.,
646 Marecal, V., Peuch, V.-H., Richter, A., Schultz, M. G., Stein, O., and Tsikerdekis, A., 2015.
647 Tropospheric chemistry in the Integrated Forecasting System of ECMWF, *Geosci. Model*
648 *Dev.*, 8, 975-1003, doi:10.5194/gmd-8-975-2015

649

650 Galmarini, S., Koffi, B., Solazzo, E., Keating, T., Hogrefe, C., Schulz, M., Benedictow, A.,
651 Griesfeller, J. J., Janssens-Maenhout, G., Carmichael, G., Fu, J., and Dentener, F.: Technical
652 note: Coordination and harmonization of the multi-scale, multi-model activities HTAP2,
653 AQMEI3, and MICS-Asia3: simulations, emission inventories, boundary conditions, and



- 654 model output formats, Atmos. Chem. Phys., 17, 1543-1555, [https://doi.org/10.5194/acp-17-](https://doi.org/10.5194/acp-17-1543-2017)
655 1543-2017, 2017.
- 656 Galmarini S, Bianconi R, Appel W, Solazzo E, Mosca S, Grossi P, et al (2012) ENSEMBLE
657 and AMET: Two systems and approaches to a harmonized, simplified and efficient facility
658 for air quality models development and evaluation. Atmos Environ 53: 51-59.
- 659 Galmarini, S., Kioutsioukis, I., and Solazzo, E.: E pluribus unum*: ensemble air quality
660 predictions, Atmos. Chem. Phys., 13, 7153-7182, <https://doi.org/10.5194/acp-13-7153-2013>,
661 2013.
- 662 Giordano, L., Brunner, D., Flemming, J., Hogrefe, C., Im, U., Bianconi, R., Badia, A.,
663 Balzarini, A., Baro, R., Chemel, C., Curci, G., Forkel, R., Jimenez-Guerrero, P., Hirtl, M.,
664 Hodzic, A., Honzak, L., Jorba, O., Knote, C., Kuenen, J.J.P., Makar, P.A., Manders-Groot,
665 A., Neal, L., Perez, J.L., Pirovano, G., Pouliot, G., San Jose, R., Savage, N., Schroder, W.,
666 Sokhi, R.S., Syrakov, D., Torian, A., Tuccella, P., Werhahn, J., Wolke, R., Yahya, K.,
667 Žabkar, R., Zhang, Y., Galmarini, S., 2015. Assessment of the MACC reanalysis and its
668 influence as chemical boundary conditions for regional air quality modeling in AQMEII-2.
669 Atmospheric Environment, 115, 371-388.
- 670 Hogrefe, C., Liu, P., Pouliot, G., Mathur, R., Roselle, S., Flemming, J., Lin, M., and Park, R.
671 J.: Impacts of Different Characterizations of Large-Scale Background on Simulated
672 Regional-Scale Ozone Over the Continental United States, Atmos. Chem. Phys. Discuss.,
673 <https://doi.org/10.5194/acp-2017-676>, in review, 2017
- 674 Holloway, T., Fiore, A., Hastings, M.G., 2003, Intercontinental transport of air pollution:
675 Will emerging science lead to a new hemispheric treaty?, Environ. Sci. Technol., 37, 4535 –
676 4542, doi:10.1021/es034031g.
- 677 Huang, M., Carmichael, G. R., Pierce, R. B., Jo, D. S., Park, R. J., Flemming, J., Emmons, L.
678 K., Bowman, K. W., Henze, D. K., Davila, Y., Sudo, K., Jonson, J. E., Tronstad Lund, M.,
679 Janssens-Maenhout, G., Dentener, F. J., Keating, T. J., Oetjen, H., and Payne, V. H.: Impact
680 of intercontinental pollution transport on North American ozone air pollution: an HTAP
681 phase 2 multi-model study, Atmos. Chem. Phys., 17, 5721-5750, [https://doi.org/10.5194/acp-](https://doi.org/10.5194/acp-17-5721-2017)
682 17-5721-2017, 2017.
- 683 Husar, R.B., Tratt, D.M., Schichtel, D.M., Falke, S.R., Li, F., Jaffe, D., Gassó, S., Gill, T.,
684 Laulainen, N. S., Lu, F., Reheis, M.C., Chun, Y., Westphal, D., Holben, B.N., Gueymard, C.,
685 McKendry, I., Kuring, N., Feldman, G.C., McClain, C., Frouin, R.J., Merrill, J., DuBois, D.,
686 Vignola, F., Murayama, T., Nickovic, S., Wilson, W. E., Sassen, K., Sugimoto, N., Malm,
687 W.C., 2001. Asian dust events of April 1998. J. Geophys. Res., 106 (D16), 18317 – 18330,
688 doi:10.1029/2000JD900788.
- 689 Huszar, P., Belda, M., and Halenka, T.: On the long-term impact of emissions from central
690 European cities on regional air quality, Atmos. Chem. Phys., 16, 1331-1352,
691 <https://doi.org/10.5194/acp-16-1331-2016>, 2016.



- 692 Im, U., Brandt, J., Geels, C., Hansen, K.M., Christensen, J.H., Andersen, M.S., Solazzo, E.,
693 Kioutsioukis, I., Alyuz, U., Balzarini, A., Baro, R., Bellasio, R., Bianconi, R., Bieser, J.,
694 Colette, A., Curci, G., Farrow, A., Flemming, J., Fraser, A., Jimenez-Guerrero, P., Kai-Chai,
695 L., Kitwiroon, N., Pirovano, G., Pozzoli, L., Prank, M., Rose, R., Sokhi, R., Tuccella, P.,
696 Unal, A., Vivanco, M.G., West, J., Yardwood, G., Hogrefe, C., Galmarini, S., 2017. Air
697 pollution impacts on human health and the associated external costs over Europe and the
698 United States as calculated by a multi-model ensemble in frame of AQMEII3, Atmospheric
699 Chemistry and Physics, Under Review.
- 700 Im, U., Bianconi, R., Solazzo, E., Kioutsioukis, I., Badia, A., Balzarini, A., Baro, R.,
701 Bellasio, R., Brunner, D., Chemel, C., Curci, G., Denier van der Gon, H.A.C., Flemming, J.,
702 Forkel, R., Giordano, L., Jimenez-Guerrero, P., Hirtl, M., Hodzic, A., Honzak, L., Jorba, O.,
703 Knote, C., Makar, P.A., Manders-Groot, A., Neal, L., Perez, J.L., Pirovano, G., Pouliot, G.,
704 San Jose, R., Savage, N., Schroder, W., Sokhi, R.S., Syrakov, D., Torian, A., Tuccella, P.,
705 Werhahn, K., Wolke, R., Yahya, K., Zabkar, R., Zhang, Y., Zhang, J., Hogrefe, C.,
706 Galmarini, S., 2015b. Evaluation of operational online-coupled regional air quality models
707 over Europe and North America in the context of AQMEII phase 2. Part II: Particulate
708 Matter. Atmospheric Environment, 115, 421-441.
- 709 Im, U., Bianconi, R., Solazzo, E., Kioutsioukis, I., Badia, A., Balzarini, A., Baro, R.,
710 Bellasio, R., Brunner, D., Chemel, C., Curci, G., Flemming, J., Forkel, R., Giordano, L.,
711 Jimenez-Guerrero, P., Hirtl, M., Hodzic, A., Honzak, L., Jorba, O., Knote, C., Kuenen, J.J.P.,
712 Makar, P.A., Manders-Groot, A., Neal, L., Perez, J.L., Pirovano, G., Pouliot, G., San Jose, R.,
713 Savage, N., Schroder, W., Sokhi, R.S., Syrakov, D., Torian, A., Werhahn, K., Wolke, R.,
714 Yahya, K., Zabkar, R., Zhang, Y., Zhang, J., Hogrefe, C., Galmarini, S., 2015a. Evaluation of
715 operational online-coupled regional air quality models over Europe and North America in the
716 context of AQMEII phase 2. Part I: Ozone. Atmospheric Environment, 115, 404-420.
- 717 Im, U. and Kanakidou, M.: Impacts of East Mediterranean megacity emissions on air quality,
718 Atmos. Chem. Phys., 12, 6335-6355, <https://doi.org/10.5194/acp-12-6335-2012>, 2012.
- 719 Jaffe, D., Bertschi, I., Jaeglé, L., Novelli, P., Reid, J.S., Tanimoto, H., Vingarzan, R.,
720 Westphal, D.L., 2004. Long-range transport of Siberian biomass burning emissions and
721 impact on surface ozone in western North America. Geophys. Res. Lett., 31, L16106,
722 doi:10.1029/2004GL020093.
- 723 Janssens-Maenhout, G., Crippa, M., Guizzardi, D., Dentener, F., Muntean, M., Pouliot, G.,
724 Keating, T., Zhang, Q., Kurokawa, J., Wankmüller, R., Denier van der Gon, H., Kuenen, J. J.
725 P., Klimont, Z., Frost, G., Darras, S., Koffi, B., and Li, M.: HTAP_v2.2: a mosaic of regional
726 and global emission grid maps for 2008 and 2010 to study hemispheric transport of air
727 pollution, Atmos. Chem. Phys., 15, 11411–11432, doi:10.5194/acp-15-11411-2015, 2015.
- 728 Jiménez, P., Parra, R., and Baldasano, J. M.: Influence of initial and boundary conditions for
729 ozone modeling in very complex terrains: a case study in the northeastern Iberian Peninsula,
730 Environ. Modell. Softw., 22, 1294–1306, 2007.



- 731 Jonson, J.E., Schulz, M., Emmons, L., Flemming, J., Henze, D., Sudo, K., Lund, M.T., Lin,
732 M., Benedictow, A., Koffi, B., Eckhart, P., Dentener, F., Keating, T., 2017. The effects of
733 intercontinental emission sources on European air pollution levels. In preparation for Atmos.
734 Chem. Phys.
- 735 Kioutsioukis, I., Im, U., Solazzo, E., Bianconi, R., Badia, A., Balzarini, A., Baró, R.,
736 Bellasio, R., Brunner, D., Chemel, C., Curci, G., Denier van der Gon, H., Flemming, J.,
737 Forkel, R., Giordano, L., Jiménez-Guerrero, P., Hirtl, M., Jorba, O., Manders-Groot, A.,
738 Neal, L., Pérez, J. L., Pirovano, G., San Jose, R., Savage, N., Schroder, W., Sokhi, R. S.,
739 Syrakov, D., Tuccella, P., Werhahn, J., Wolke, R., Hogrefe, C., and Galmarini, S.: Improving
740 the deterministic skill of air quality ensembles, Atmos. Chem. Phys., 16, 15629-15652.
- 741 Li, Q., Jacob, D.J., Bey, I., Palmer, P.I., Duncan, B.N., Field, B.D., Martin, R.V., Fiore,
742 A.M., Yantosca, R.M., Parrish, D.D., Simmonds, P.G., Oltmans, S.J., 2002. Transatlantic
743 transport of pollution and its effects on surface ozone in Europe and North America. J.
744 Geophys. Res, 107, D13, 4166, 10.1029/2001JD001422.
- 745 Liang, C., Silva, R.A., West, J.J., Emmons, L., Jonson, J.E., Bian, H., Pan, X., Chin, M.,
746 Henze, D., Lund, M.T., Sudo, K., Sekiya, T., Takemura, T., Flemming, J., Park, R., Lin, M.,
747 Pierce, R.B., Lenzen, A., Kucsera, T., Folberth, G., 2017. Multi-model estimates of
748 premature human mortality due to intercontinental transport of air pollution. Atmospheric
749 Chemistry and Physics, In preparation for Atmos. Chem. Phys.
- 750 Mason, R., Zubrow, A., Eyth, A., 2007. Technical Support Document (TSD) Preparation of
751 Emissions Inventories for the Version 5.0, 2007 Emissions Modeling Platform, available at:
752 <https://www.epa.gov/air-emissions-modeling/2007-version-50-technical-support-document>,
753 last access: 24 May 2017.
- 754 Mathur, R.: Estimating the impact of the 2004 Alaskan forest fires on episodic particulate
755 matter pollution over the eastern United States through assimilation of satellite-derived
756 aerosol optical depths in a regional air quality model, J. Geophys. Res., 113, D17302,
757 doi:10.1029/2007JD009767, 2008.
- 758 Pouliot, G., Denier van der Gon, H., Kuenen, J., Makar, P., Zhang, J., Moran, M., 2015.
759 Analysis of the emission inventories and model-ready emission datasets of Europe and North
760 America for phase 2 of the AQMEII project. Atmos. Environ. 115, 345-360.
- 761 Rao, S., Mathur, R., Hogrefe, C. Keating, T., Dentener, F., and Galmarini, S.: Path Forward
762 for the Air Quality Model Evaluation International Initiative (AQMEII), EM, Air And Waste
763 Management Associations Magazine For Environmental Managers, 7, 38–41, 2012.
- 764 Rudich, Y., Kaufman, Y. J., Dayan, U., Yu, H., and Kleidman, R. G.: Estimation of
765 transboundary transport of pollution aerosols by remote sensing in the eastern Mediterranean,
766 J. Geophys. Res., 113, D14S13, doi:10.1029/2007JD009601, 2008.
- 767 Solazzo, E., Bianconi, R., Hogrefe, C., Curci, G., Alyuz, U., Balzarini, A., Baró, R., Bellasio,
768 R., Bieser, J., Brandt, J., Christensen, J. H., Colette, A., Francis, X., Fraser, A., Garcia



- 769 Vivanco, M., Jiménez-Guerrero, P., Im, U., Manders, A., Nopmongcol, U., Kitwiroon, N.,
770 Pirovano, G., Pozzoli, L., Prank, M., Sokhi, R. S., Tuccella, P., Unal, A., Yarwood, G., and
771 Galmarini, S., 2017b. Evaluation and Error Apportionment of an Ensemble of Atmospheric
772 Chemistry Transport Modelling Systems: Multi-variable Temporal and Spatial Breakdown,
773 Atmos. Chem. Phys., 17, 3001-3054.
- 774 Solazzo, E., Hogrefe, C., Colette, A., Garcia-Vivanco, M., Galmarini, S., 2017a. Advanced
775 error diagnostics of the CMAQ and Chimere modelling systems within the AQMEII3 model
776 evaluation framework. Atmos. Chem. Phys., 17, 10435-10465, <https://doi.org/10.5194/acp-17-10435-2017>.
- 778 Solazzo, E., Riccio, A., Kioutsioukis, I., Galmarini, S., 2013b. Pauci ex tanto numero: reduce
779 redundancy in multi-model ensembles. Atmos. Chem. Phys. 13, 8315-8333.
- 780 Solazzo, E., Bianconi, R., Vautard, R., Appel, K.W., Moran, M.D., Hogrefe, C., Bessagnet,
781 B., Brandt, J., Christensen, J.H., Chemel, C., Coll, I., van der Gon, H.D., Ferreira, J., Forkel,
782 R., Francis, X.V., Grell, G., Grossi, P., Hansen, A.B., Jericevic, A., Kraljevic, L., Miranda,
783 A.I., Nopmongcol, U., Pirovano, G., Prank, M., Riccio, A., Sartelet, K.N., Schaap, M., Silver,
784 J.D., Sokhi, R.S., Vira, J., Werhahn, J., Wolke, R., Yarwood, G., Zhang, J., Rao, S.T.,
785 Galmarini, S., 2012a. Ensemble modelling of surface level ozone in Europe and North
786 America in the context of AQMEI. Atmos. Environ. 53, 60-74.
- 787 Solazzo, E., Bianconi, R., Pirovano, G., Matthias, V., Vautard, R., Moran, M.D., Appel,
788 K.W., Bessagnet, B., Brandt, J., Christensen, J.H., Chemel, C., Coll, I., Ferreira, J., Forkel,
789 R., Francis, X.V., Grell, G., Grossi, P., Hansen, A.B., Hogrefe, C., Miranda, A.I.,
790 Nopmongco, U., Prank, M., Sartelet, K.N., Schaap, M., Silver, J.D., Sokhi, R.S., Vira, J.,
791 Werhahn, J., Wolke, R., Yarwood, G., Zhang, J., Rao, S.T., Galmarini, S., 2012b.
792 Operational model evaluation for particulate matter in Europe and North America in the
793 context of AQMEII. Atmos. Environ. 53, 75-92.
- 794 Song, C.-K., Byun, D. W., Pierce, R. B., Alsaadi, J. A., Schaack, T. K., and Vukovich, F.:
795 Downscale linkage of global model output for regional chemical transport modeling: method
796 and general performance, J. Geophys. Res., 113, D08308, doi:10.1029/2007JD008951, 2008.
- 797 Stjern, C. W., Samset, B. H., Myhre, G., Bian, H., Chin, M., Davila, Y., Dentener, F.,
798 Emmons, L., Flemming, J., Haslerud, A. S., Henze, D., Jonson, J. E., Kucsera, T., Lund, M.
799 T., Schulz, M., Sudo, K., Takemura, T., and Tilmes, S.: Global and regional radiative forcing
800 from 20 % reductions in BC, OC and SO₄ – an HTAP2 multi-model study, Atmos. Chem.
801 Phys., 16, 13579-13599, <https://doi.org/10.5194/acp-16-13579-2016>, 2016.
- 802 Tang, Y., Carmichael, G. R., Thongboonchoo, N., Chai, T., Horowitz, L. W., Pierce, R. B.,
803 Al-Saadi, J. A., Pfister, G., Vukovich, J. M., Avery, M. A., Sachse, G. W., Ryerson, T. B.,
804 Holloway, J. S., Atlas, E. L., Flocke, F. M., Weber, R. J., Huey, L. G., Dibb, J. E., Streets, D.
805 G., and Brune, W. H.: Influence of lateral and top boundary conditions on regional air quality
806 prediction: a multiscale study coupling regional and global chemical transport models, J.
807 Geophys. Res., 112, D10S18, doi:10.1029/2006JD007515, 2007.



- 808 United Nations, 2007. Hemispheric transport of air pollution 2007. Air Pollution Studies No.
809 16, Interim report prepared by the Task Force on Hemispheric Transport of Air Pollution
810 acting within the framework of the Convention on Long-range Transboundary Air Pollution.
811 New York and Geneva, 2007.
- 812 Vivanco, M.G., Theobald, M.R., García-Gómez, H., Garrido, J.L., Prank, M., Aas, W.,
813 Adani, M., Alyuz, U., Andersson, C., Bellasio, R., Bessagnet, B., Bianconi, B., Bieser, J.,
814 Brandt, J., Briganti, G., Cappelletti, A., Christensen, J.H., Ciarelli, G., Colette, A., Couvidat,
815 F., Cuvelier, K., D'Isidoro, M., Flemming, J., Fraser, A., Galmarini, S., Geels, C., Hansen,
816 K.M., Hogrefe, C., Im, U., Manders, A., Mircea, M., Pay, M.-T., Pozzoli, L., Raffort, V.,
817 Roustan, Y., Solazzo, E., Tsyro, S., Tuccella, P., Unal, A., Wind, P., 2017. Modelled
818 deposition of nitrogen and sulfur in Europe estimated by 15 air quality models: Evaluation,
819 effects of changes in emissions and implications for habitat protection. In preparation for
820 Atmos. Chem. Phys.
- 821 Wilkening, K.E., Barrie, L.A., Engle, M., 2000. Atmospheric science: Trans-Pacific air
822 pollution. *Science*, 290, 65 – 67, doi:10.1126/science.290.5489.65.
- 823 World Health Organization (WHO), 2013. Review of evidence on health aspects of air
824 pollution (REVIHAAP). WHO Technical Report.



825 Table 1. Key features (meteorological/chemistry and transport models, emissions, horizontal and vertical grids) of the regional models
 826 participating to the AQMEII3 health impact study and the perturbation scenarios they performed.

Group Code	Model	Emissions ¹	Horizontal Resolution	Vertical Resolution	Europe				North America			
					BASE	GLO	NAM	EUR	BASE	GLO	EAS	NAM
DE1	COSMO-CLM/CMAQ	HTAP	24 km × 24 km	30 layers, 50 hPa	x	x	x	x	x	x	x	x
DK1	WRF/DEHM	HTAP	50 km × 50 km	29 layers, 100 hPa	x	x	x	x	x	x	x	x
ES1	WRF/CHEM	MACC	23 km × 23 km	33 layers, 50 hPa	x		x					
FI1	ECMWF/SILAM	MACC+HTAP	0.25° × 0.25°	12 layers, 13 km	x	x	x	x				
FRES1	ECMWF/CHIMERE	MACC+HTAP	0.25° × 0.25°	9 layers, 50 hPa	x	x	x	x				
IT1	WRF/CAMx	MACC	23 km × 23 km	33 layers, 50 hPa	x	x		x				
IT2	WRF/CHEM	MACC	23 km × 23 km	14 layers, 8 km	x	x						
NL1	LOTOS/EUROS	MACC	0.50° × 0.25°	4 layers, 3.5 km	x							
TR1	WRF/CMAQ	MACC	30 km × 30 km	24 layers, 10hPa	x	x	x					
UK1	WRF/CMAQ	MACC	15 km × 15 km	23 layers, 100 hPa	x	x	x	x				
UK2	WRF/CMAQ	HTAP	30 km × 30 km	23 layers, 100 hPa	x	x						
UK3	WRF/CMAQ	MACC	18 km × 18 km	35 layers, 16 km	x	x	x					
US1	WRF/CAMx	SMOKE	12 km × 12 km	29 layers, 97.5 hPa					x	x	x	x
US3	WRF/CMAQ	SMOKE	12 km × 12 km	35 layers, 50 hPa					x	x	x	x

827 ¹ MACC: Modelling group used only the MACC emissions, MACC+HTAP: Modelling group used MACC emissions for Europe and HTAP
 828 emissions over North Africa.



830 Table 2. Perturbations of global/regional anthropogenic emissions and boundary conditions in the perturbation scenarios.

	GLO	Europe		North America	
		NAM	EUR	NAM	EAS
Emissions	-20%	-	-20%	-20%	-
Boundary conditions (Emissions in the IFS model)	-20%	-20%	-20%	-20%	-20%

831

832



833 Table 3. Monthly statistics of Pearson's Correlation (r), Normalized Mean Bias (NMB : %), Normalized Mean Gross Error ($NMGE$: %) and Root
834 Mean Square Error ($RMSE$: $\mu\text{g m}^{-3}$ for Europe, while ppb for gases and $\mu\text{g m}^{-3}$ for particles for North America) calculated for each model group.

	EUROPE														NORTH AMERICA						
	DEI	DKI	ES1	FU1	FRES1	IT1	IT2	TR1	UK1	UK2	MEAN	MEDIAN	C-IFS	DEI	DKI	US1	US3	MEAN	MEDIAN	C-IFS	
O ₃	r	0.63	0.90	0.82	0.83	0.91	0.92	0.87	0.92	0.90	0.93	0.92	0.89	0.78	0.59	0.89	0.87	0.84	0.83	0.71	
	NMB	0.10	0.07	-0.14	-0.36	-0.10	0.04	0.09	0.08	-0.03	-0.04	-0.04	-0.20	0.12	0.22	0.14	-0.02	0.09	0.11	-0.10	
	NMGE	0.17	0.12	0.15	0.36	0.12	0.13	0.15	0.26	0.11	0.09	0.08	0.20	0.17	0.23	0.14	0.08	0.12	0.13	0.19	
	RMSE	12.68	8.81	11.58	23.13	9.01	8.54	10.94	17.66	8.05	6.79	5.91	6.31	14.63	6.16	9.81	5.72	3.23	4.63	5.28	7.31
NO ₂	r	0.80	0.88	0.89	0.95	0.74	0.90	0.92	0.85	0.85	0.95	0.93	0.92	0.99	0.92	0.94	0.93	0.98	0.99	0.91	
	NMB	-0.75	-0.38	-0.47	0.00	0.05	-0.29	0.58	-0.32	-0.06	-0.17	-0.24	0.07	-0.18	-0.35	0.05	0.31	-0.03	-0.02	0.41	
	NMGE	0.75	0.38	0.47	0.20	0.23	0.29	0.30	0.58	0.32	0.17	0.24	0.20	0.18	0.35	0.10	0.31	0.06	0.02	0.41	
	RMSE	9.38	5.41	6.00	2.89	3.44	4.43	7.39	4.65	4.65	2.74	2.70	3.49	2.59	1.01	2.05	0.62	1.77	0.40	0.26	2.30
CO	r	0.83	0.76	0.74	0.88	0.82	0.84	0.79	0.87	0.63	0.72	0.92	0.84	0.91	0.79	0.74	0.74	0.73	0.88	0.82	0.80
	NMB	-0.42	-0.42	-0.44	-0.27	-0.32	-0.38	-0.44	-0.20	-0.41	-0.43	-0.33	-0.38	-0.25	-0.19	-0.07	-0.06	-0.04	-0.07	-0.07	0.17
	NMGE	0.42	0.42	0.44	0.27	0.32	0.38	0.44	0.21	0.41	0.43	0.33	0.38	0.25	0.19	0.11	0.08	0.08	0.07	0.17	
	RMSE	128.62	134.31	132.78	89.99	107.81	128.14	135.83	70.04	130.21	135.82	106.98	123.61	84.73	40.27	24.90	22.44	20.51	19.94	20.41	37.30
SO ₂	r	0.85	0.90	0.88	0.86	0.87	0.86	0.54	0.83	0.83	0.93	0.92	0.70	0.79	0.81	0.80	0.78	0.87	0.78	0.04	
	NMB	-0.01	-0.47	-0.65	-0.20	-0.16	-0.30	-0.55	0.04	-0.13	0.20	-0.19	-0.10	0.41	-0.46	-0.42	0.07	-0.13	-0.19	-0.13	0.35
	NMGE	0.24	0.48	0.65	0.28	0.22	0.31	0.55	0.28	0.19	0.28	0.21	0.12	0.45	0.46	0.42	0.11	0.13	0.19	0.13	0.35
	RMSE	0.92	1.47	2.03	0.95	0.80	1.23	1.71	1.14	0.86	1.05	0.76	0.58	1.39	1.27	1.18	0.32	0.40	0.53	0.40	1.02
PM ₁₀	r	0.86	0.82	0.17	0.41	0.82	0.60	0.10	0.52	0.71	0.87	0.73	-0.74	-0.31	-0.47	NA	0.07	0.47	-0.07	0.02	
	NMB	-0.71	-0.59	-0.47	-0.42	-0.51	-0.20	-0.48	-0.25	-0.47	-0.42	-0.45	-0.62	-0.67	-0.84	NA	-0.25	-0.44	-0.46	-0.86	
	NMGE	0.71	0.59	0.47	0.42	0.51	0.25	0.48	0.26	0.47	0.42	0.45	0.62	0.67	0.84	NA	0.27	0.44	0.46	0.86	
	RMSE	20.43	18.25	16.16	14.67	15.74	9.78	16.48	10.45	14.78	13.72	13.15	14.63	19.87	20.42	25.09	NA	9.85	13.51	14.74	25.58
PM _{2.5}	r	0.89	0.86	0.24	0.58	0.84	0.75	0.11	0.62	0.77	0.89	0.82	-0.73	0.52	0.02	NA	0.54	0.61	0.56	0.18	
	NMB	-0.64	-0.47	-0.27	-0.27	-0.36	-0.19	-0.48	-0.17	-0.40	-0.28	-0.32	-0.33	-0.59	-0.63	-0.14	NA	-0.15	-0.08	-0.39	
	NMGE	0.64	0.47	0.35	0.30	0.36	0.24	0.49	0.24	0.41	0.30	0.32	0.33	0.59	0.63	0.20	NA	0.22	0.15	0.40	
	RMSE	11.95	9.92	9.20	8.02	8.06	6.57	11.65	6.82	8.65	7.15	7.51	7.99	12.97	6.79	2.40	NA	2.78	1.92	1.41	5.04



835 Table 4. Annual mean absolute differences (ppb for gases and $\mu\text{g m}^{-3}$ for particles) between the base case and the different emission perturbation
 836 scenarios as calculated by the different model groups over the European domain.

Pollutant	Scenario	DE1	DK1	ES1	FII	IT1	IT2	TR1	UK1	UK2	FRES1	All Mean	Common Mean
O ₃	GLO	-1.54	-0.71		-0.40	-0.37	-0.63	2.83	-0.83	-0.79	-0.63	-0.34	-0.82
	NAM	-0.28	-0.24	0.77	-0.13			-0.30	-0.22		-0.22	-0.09	-0.22
	EUR	-0.77	0.14		0.09	0.43			0.06		0.12	0.01	-0.07
NO ₂	GLO	-0.28	-0.72		-1.20	-0.93	-0.95	-1.93	-0.75	-1.10	-0.89	-0.97	-0.77
	NAM	0.00	0.01	0.17	0.00	0.00		0.01				0.03	0.00
CO	EUR	-0.30	-0.69		-1.05	-0.85			-0.70		-0.89	-0.75	-0.73
	GLO	-15.97	-14.03		-21.10	-18.13	-15.04	-26.01	-12.83	-16.94	-16.11	-17.35	-16.01
	NAM	-1.50	-1.71	3.26	-1.41			-1.35	-1.33		-1.55	-0.80	-1.50
SO ₂	EUR	-10.49	-6.91		-14.63	-10.11			-7.87		-9.51	-9.92	-9.88
	GLO	-0.23	-0.12		-0.17	-0.17	-0.11	-0.23	-0.20	-0.28	-0.15	-0.18	-0.17
	NAM	0.00	0.00	0.03	0.00	0.00		0.00	0.00		0.00	0.00	0.00
PM ₁₀	EUR	-0.23	-0.10		-0.14	-0.13			-0.16		-0.15	-0.15	-0.16
	GLO	-1.47	-1.90		-2.52	-2.97	-1.58	-3.58	-2.32	-2.81	-2.27	-2.38	-2.10
	NAM	-0.01	-0.09	0.00	-0.02			-0.04	-0.03		-0.04	-0.03	-0.04
PM _{2.5}	EUR	-2.03	-1.53		-2.20	-2.46			-1.96		-2.07	-2.04	-1.96
	GLO	-1.30	-1.76		-2.15	-2.56	-1.33	-2.79	-1.78	-2.44	-2.10	-2.02	-1.82
	NAM	0.01	-0.05	0.00	-0.02			-0.03	-0.02		-0.04	-0.02	-0.02
EUR	-1.29	-1.42		-1.82	-2.05			-1.47		-1.89	-1.66	-1.58	



838 Table 5. Annual mean absolute differences (ppb for gases and $\mu\text{g m}^{-3}$ for particles) between the base case and the different emission perturbation
 839 scenarios as calculated by the different model groups over the North American domain.

Pollutant	Scenario	DEI	DK1	US1	US3	All Mean	Common Mean
O ₃	GLO	-1.70	-1.42	-1.41	-1.03	-1.39	-1.39
	NAM	-0.92	-0.66		-0.36	-0.65	-0.65
	EAS	-0.35	-0.24	-0.23	-0.19	-0.25	-0.26
NO ₂	GLO	-0.35	-0.63	-1.07	-1.20	-0.81	-0.73
	NAM	-0.36	-0.62		-1.17	-0.71	-0.71
CO	EAS	0.00	0.00	0.00	-0.01	0.00	0.00
	GLO	-9.31	-20.48	-22.12	-25.01	-19.23	-18.27
	NAM	-3.84	-13.35		-19.87	-12.35	-12.35
SO ₂	EAS	-2.60	-4.16	-3.64	-3.07	-3.37	-3.28
	GLO	-0.33	-0.32	-0.48	-0.25	-0.34	-0.30
	NAM	-0.33	-0.32		-0.48	-0.37	-0.37
PM ₁₀	EAS	0.00	0.00		0.00	0.00	0.00
	GLO	-2.26	-0.66		-4.24	-2.39	-2.39
	NAM	-2.02	-0.59		-4.19	-2.27	-2.27
PM _{2.5}	EAS	-0.56	-0.05		-0.03	-0.21	-0.21
	GLO	-0.60	-1.67		-2.29	-1.52	-1.52
	NAM	-0.62	-1.56		-2.24	-1.47	-1.47
EAS	0.01	-0.04		-0.03	-0.02	-0.02	

840

841

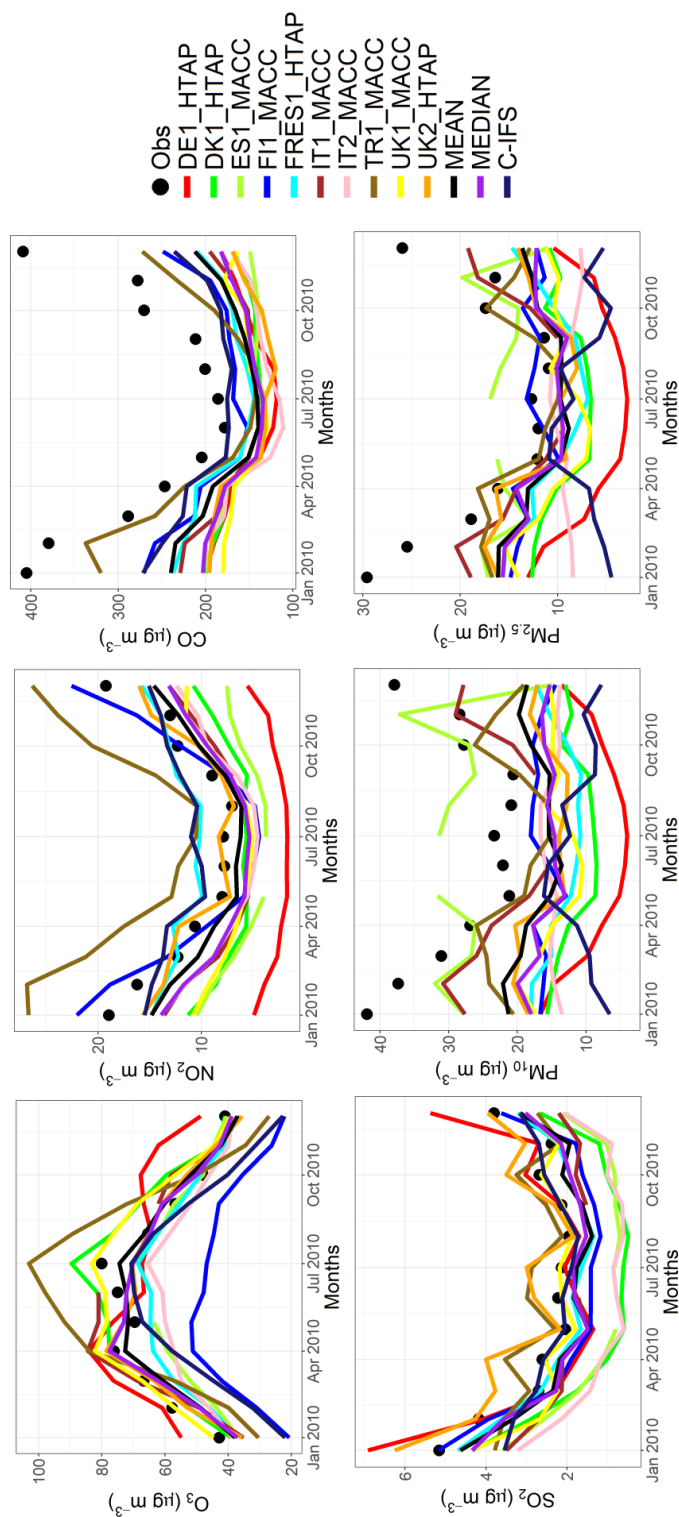


842 Table 6. Annual mean RERER values calculated for the multi-model mean ensembles over Europe and North America.

	O ₃	NO ₂	CO	SO ₂	PM ₁₀	PM _{2.5}
	EUROPE					
DE1	0.44	-0.09	0.44	0.02	0.01	0.01
DK1	0.85	0.23	0.63	0.37	0.17	0.28
FI1	0.76	-0.01	0.40	0.01	0.02	0.02
FRES1	0.78	0.15	0.56	0.30	0.20	0.20
IT1	1.10	0.34	0.93	0.42	0.27	0.26
UK1	0.92	0.35	0.52	0.43	0.33	0.34
MMM	0.77	0.18	0.55	0.27	0.18	0.19
	NORTH AMERICA					
DE1	0.77	0.12	0.73	0.07	0.09	0.12
DK1	0.93	0.06	0.90	0.15	0.07	0.12
US3	0.54	0.02	0.47	0.11	0.08	0.10
MMM	0.75	0.05	0.71	0.11	0.08	0.11

843

844



845 Fig. 1. Observed and simulated monthly mean air pollutant levels, averaged over the monitoring stations over Europe.

846

847

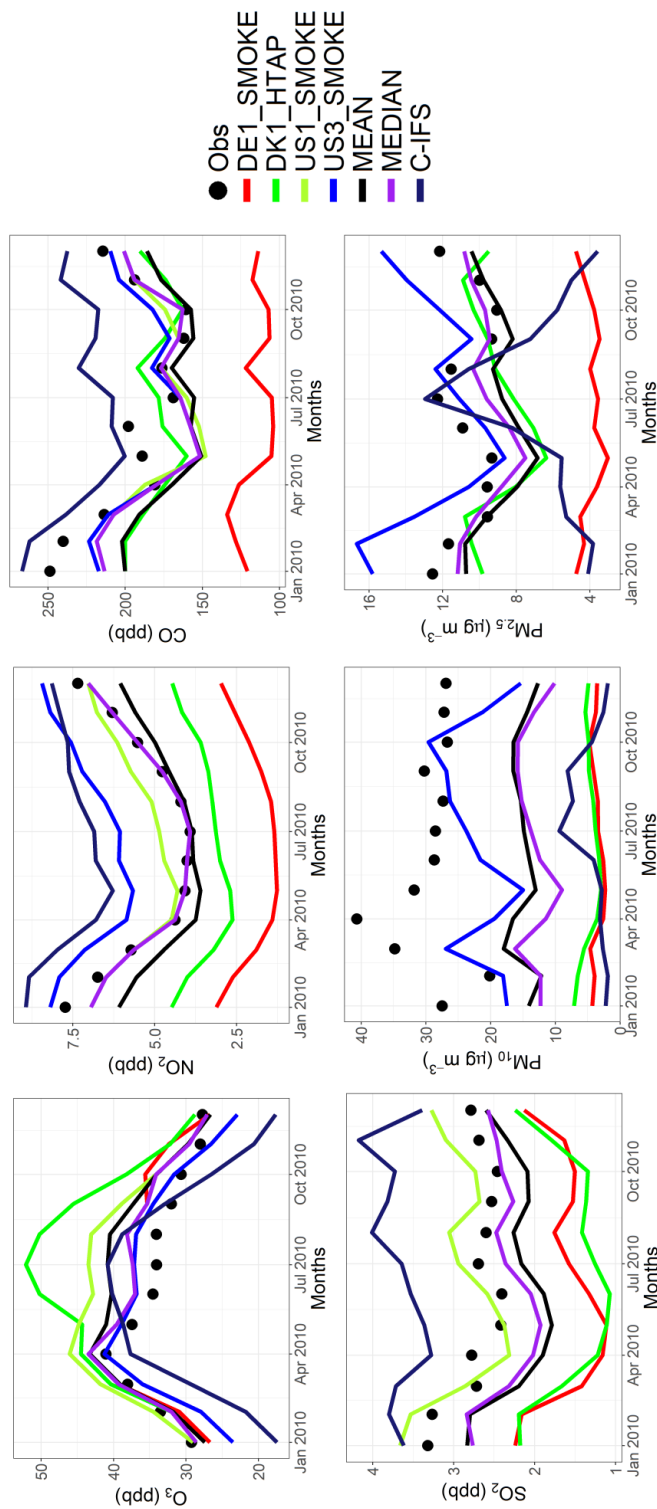


Fig.2. Observed and simulated monthly mean air pollutant levels, averaged over the monitoring stations over North America.

848

849

850

851

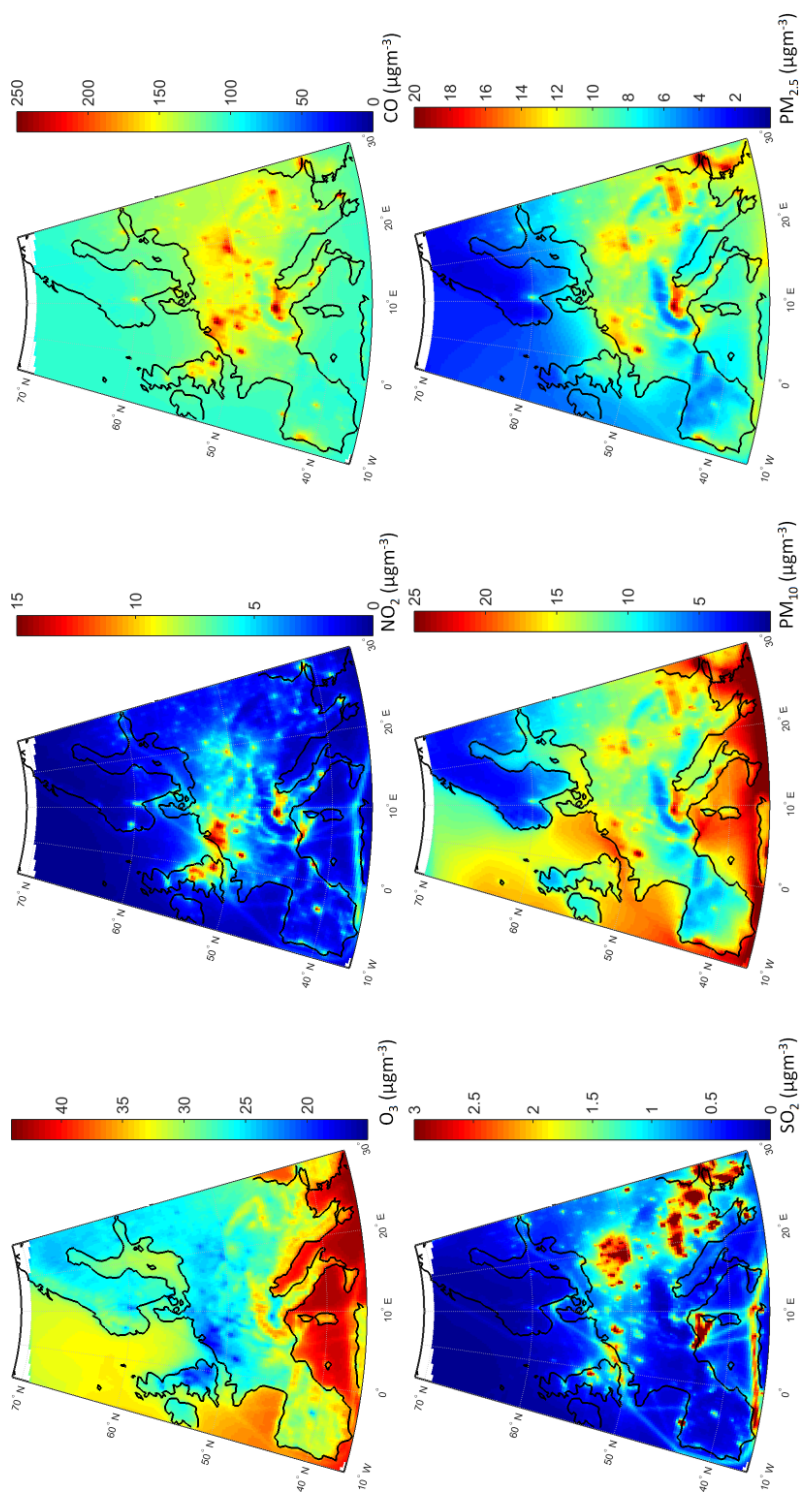
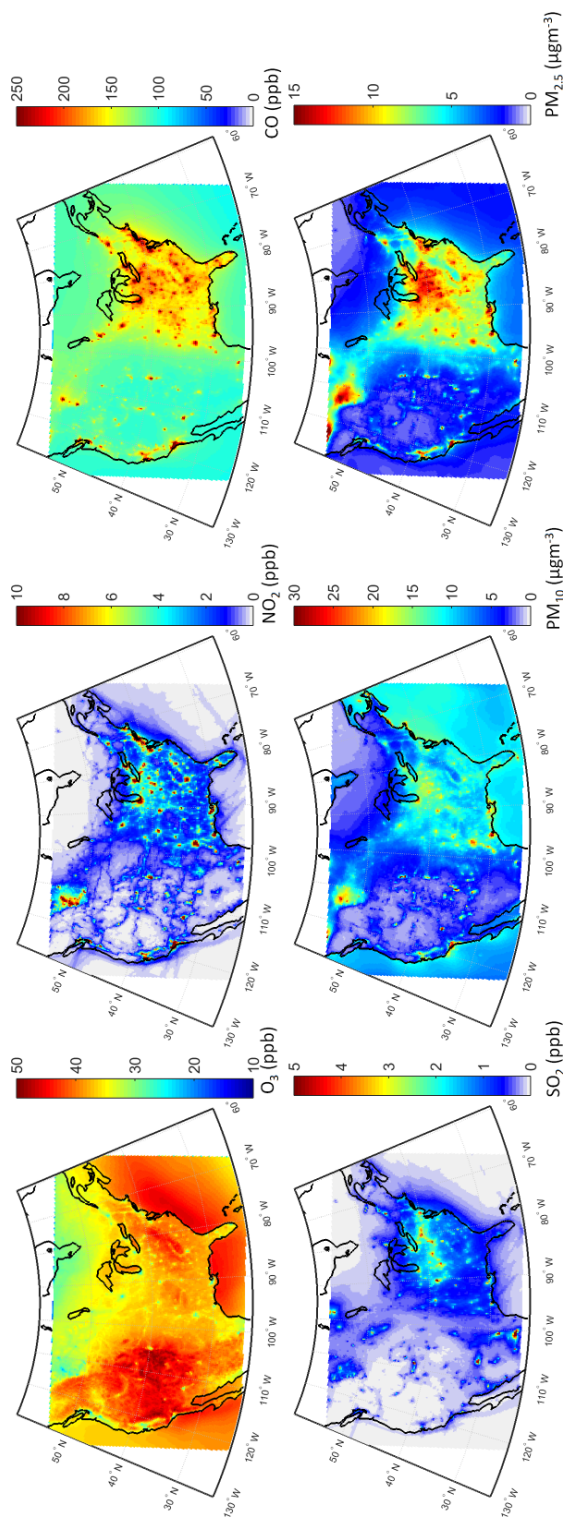


Fig.3. Multi-model mean air pollutant levels over Europe as simulated in the base case.

852

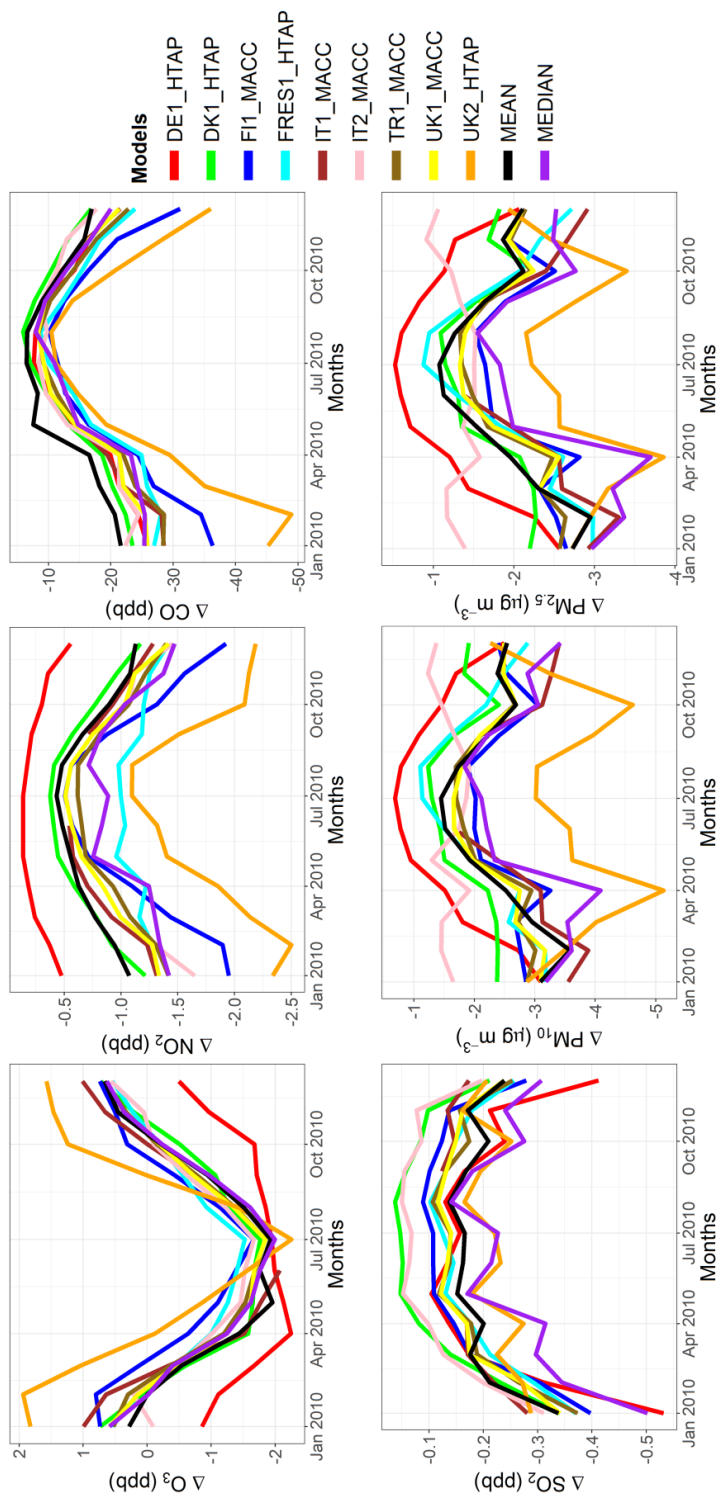
853
854

855



856 Fig. 4. Multi-model mean air pollutant levels over North America as simulated in the base case.
857

858



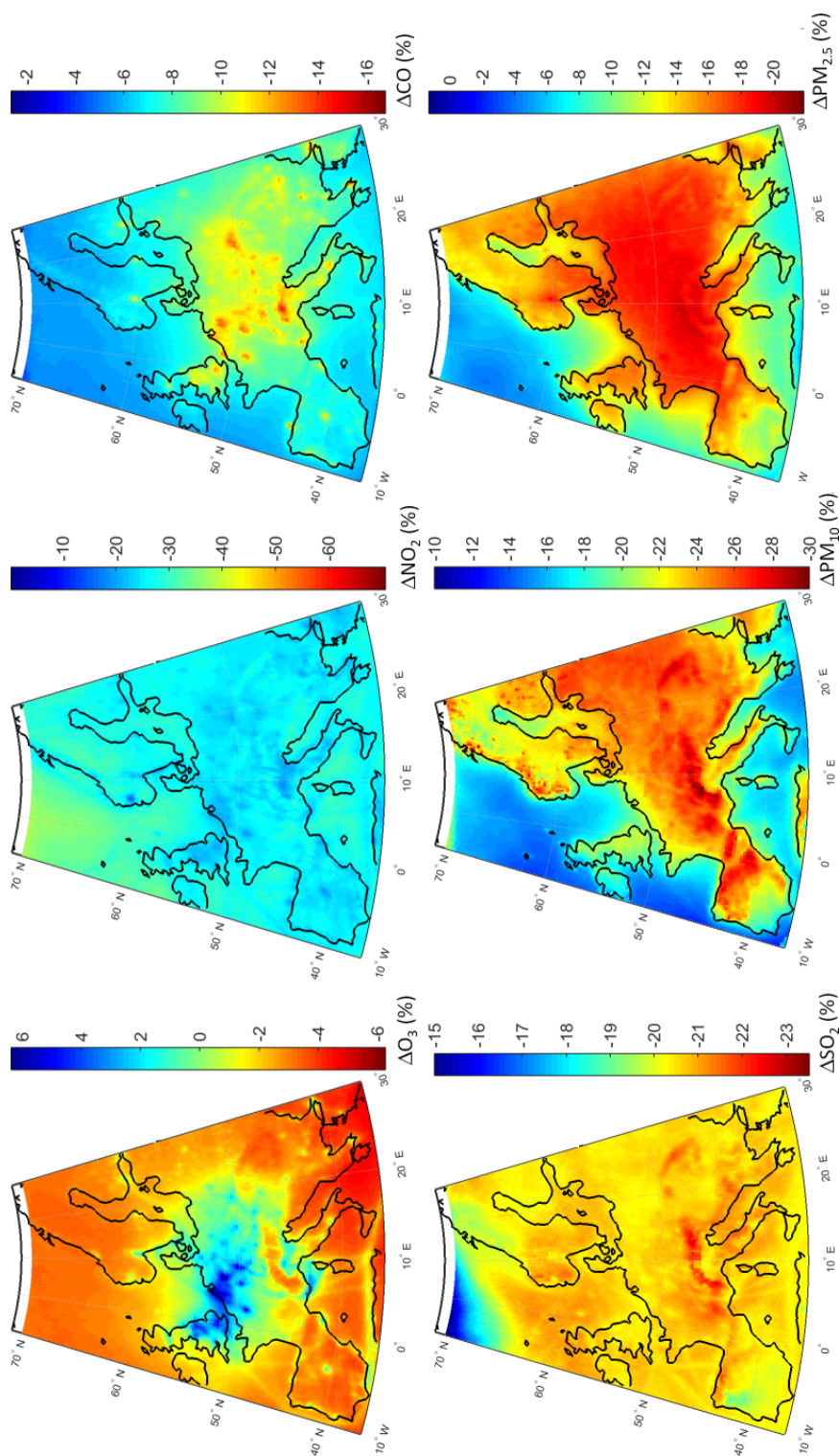
860 Fig.5. Absolute impact of the 20% reduction of the global anthropogenic emissions over Europe (GLO_{EUR}-BASE_{EUR}).

859

860

861

862

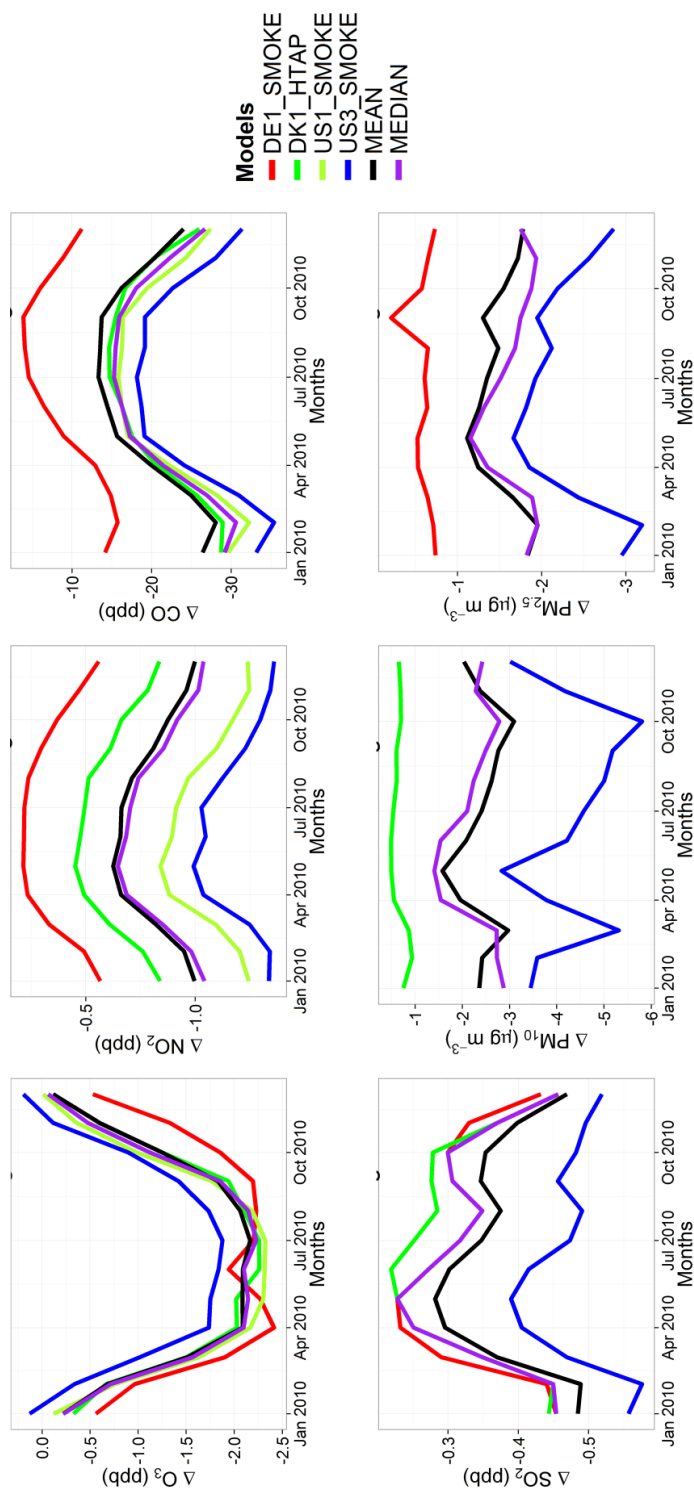


863

864 Fig.6. Spatial distribution of the annual mean relative differences between the global perturbation scenario and the base case over Europe as
865 simulated by the multi-model mean ensemble.

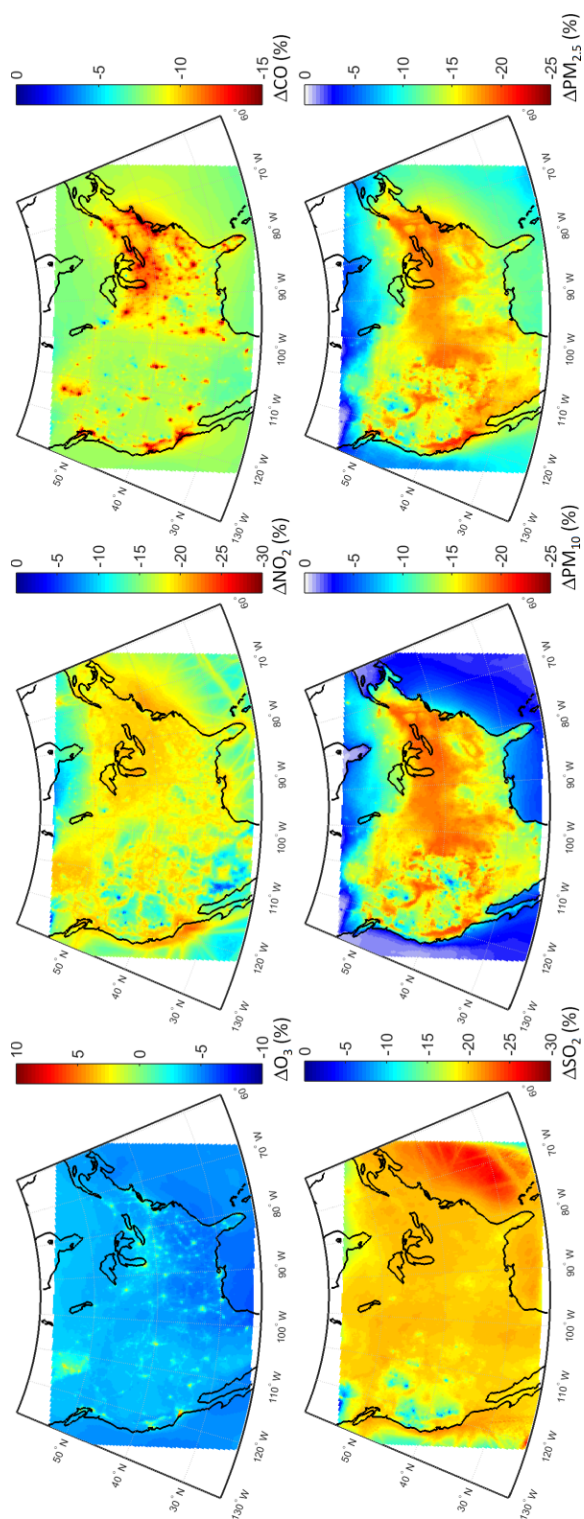


866



867
 868 Fig. 7. Absolute impact of the 20% reduction of the global anthropogenic emissions over North America (GLO_{NAM}-BASE_{NAM}).
 869

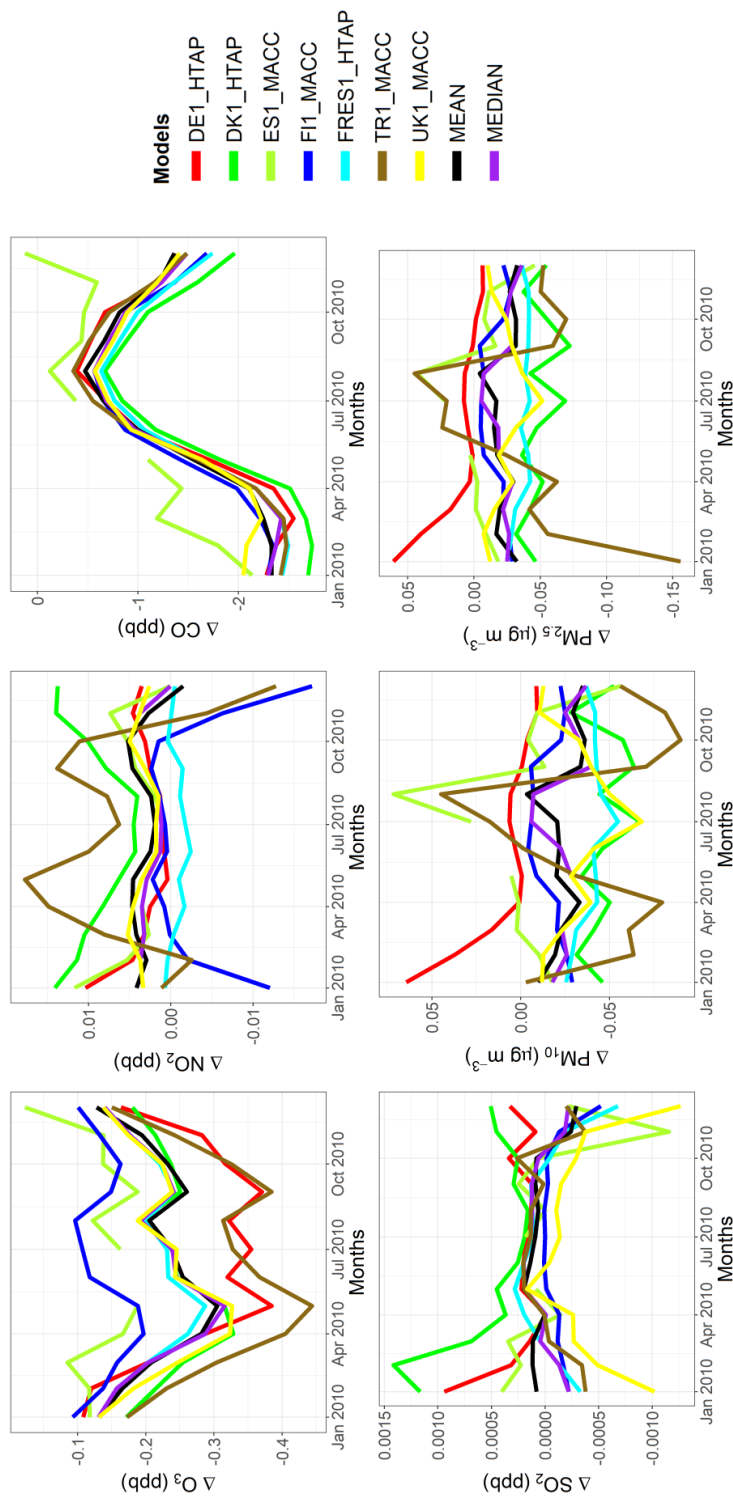
34



870

871 Fig. 8. Spatial distribution of the annual mean relative differences between the global perturbation scenario and the base case over North America
872 as simulated by the multi-model mean ensemble.

873

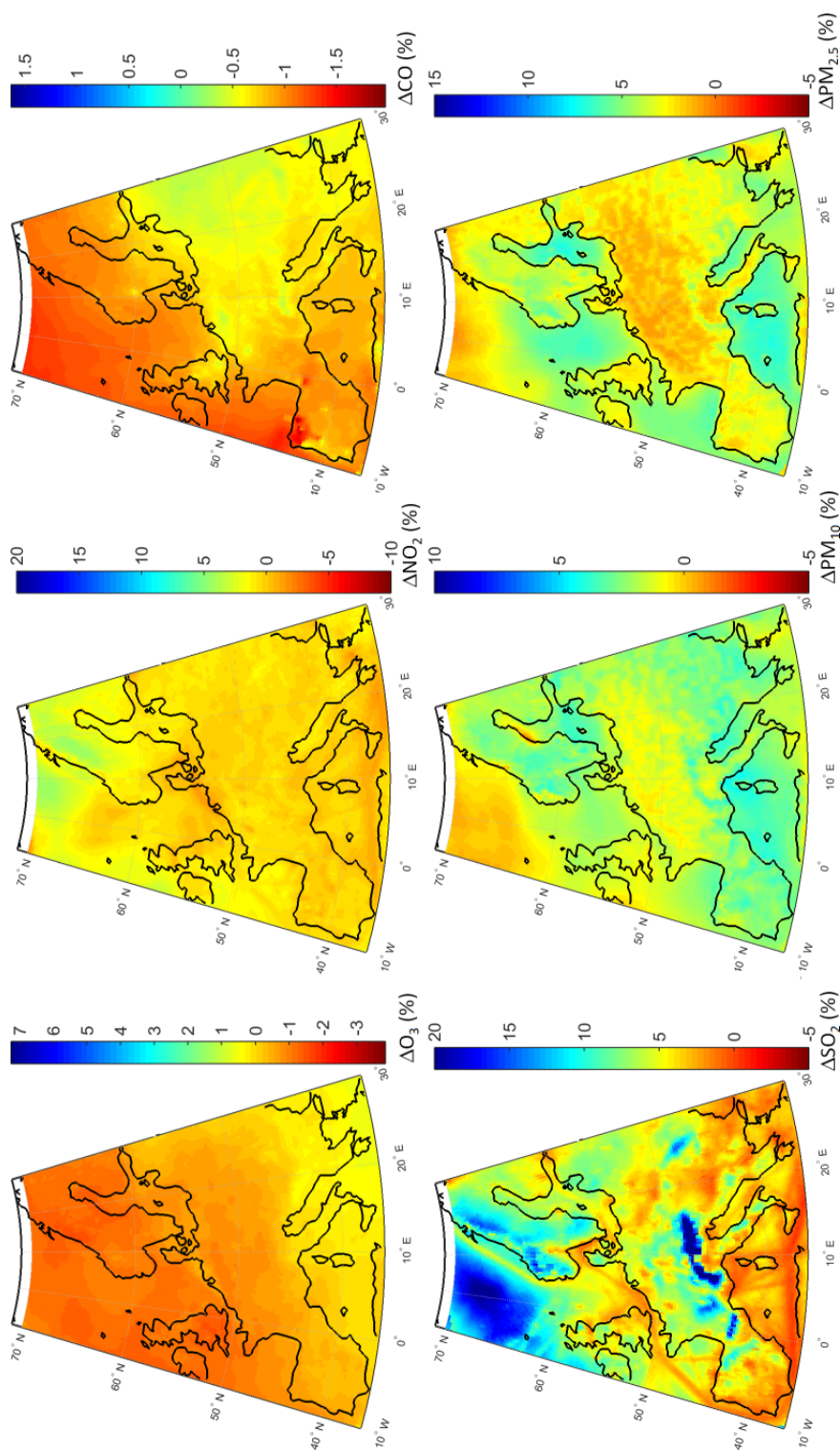


874

875

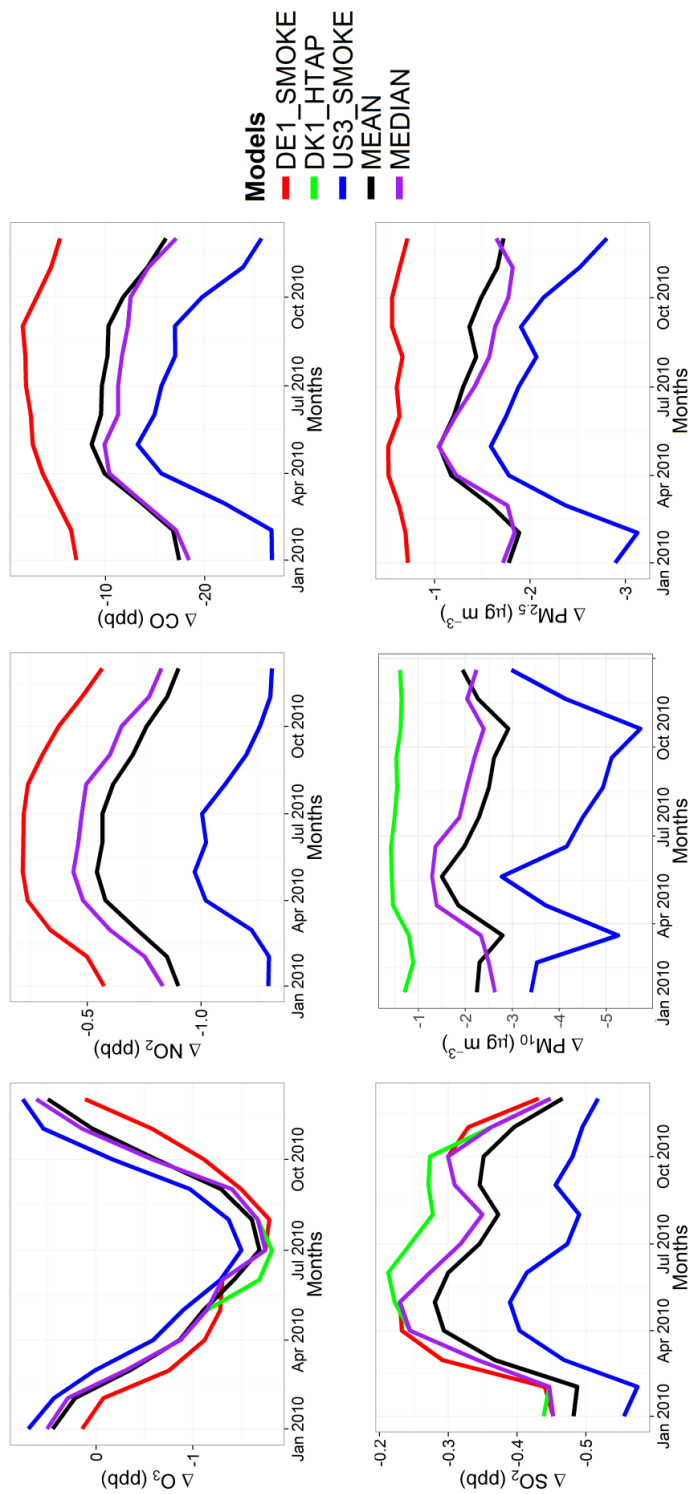
876 Fig.9. Absolute impact of the 20% reduction of the North American anthropogenic emissions over Europe (NAM_{EUR}-BASE_{EUR}).

877



878

879 Fig.10. Spatial distribution of the annual mean relative differences between the North American emissions perturbation scenario and the base
880 case over Europe as simulated by the multi-model mean ensemble.



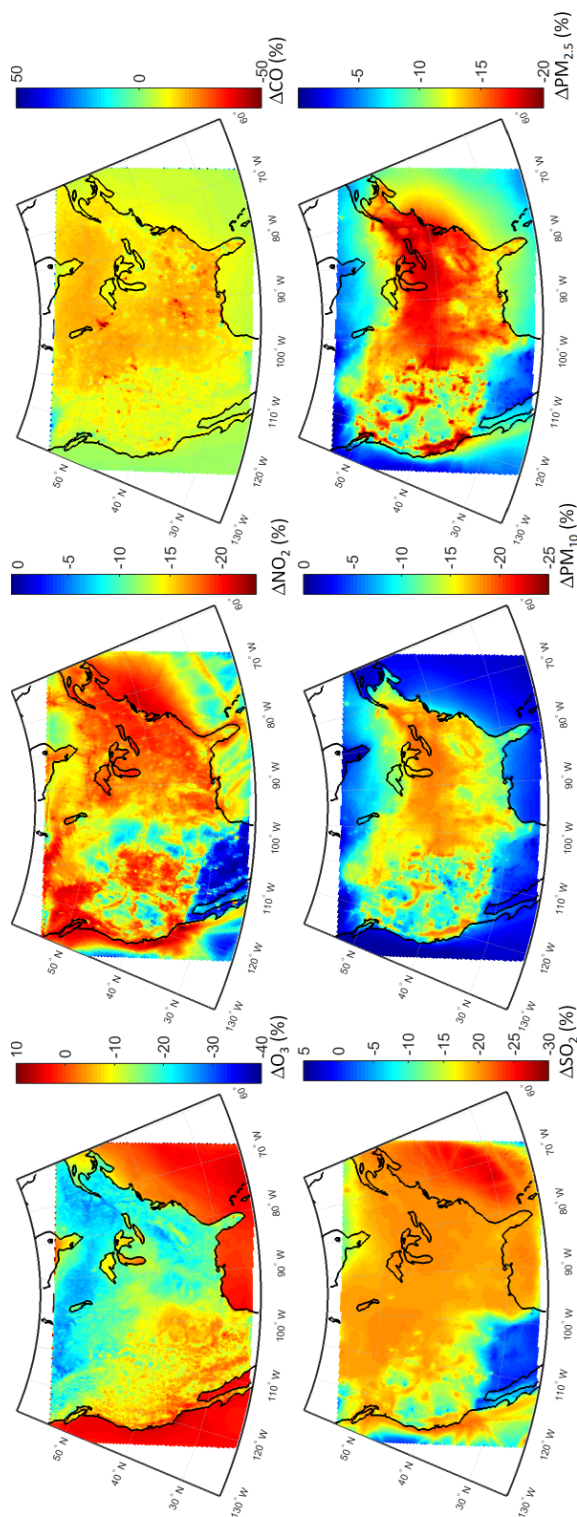
881 Fig. 11. Absolute impact of the 20% reduction of the North American anthropogenic emissions over North America (GLO_{NAM}-BASE_{NAM}).

882

883

884

885



886

887 Fig. 12. Spatial distribution of the annual mean relative differences between the North American emissions perturbation scenario and the base
888 case over North America as simulated by the multi-model mean ensemble.

889

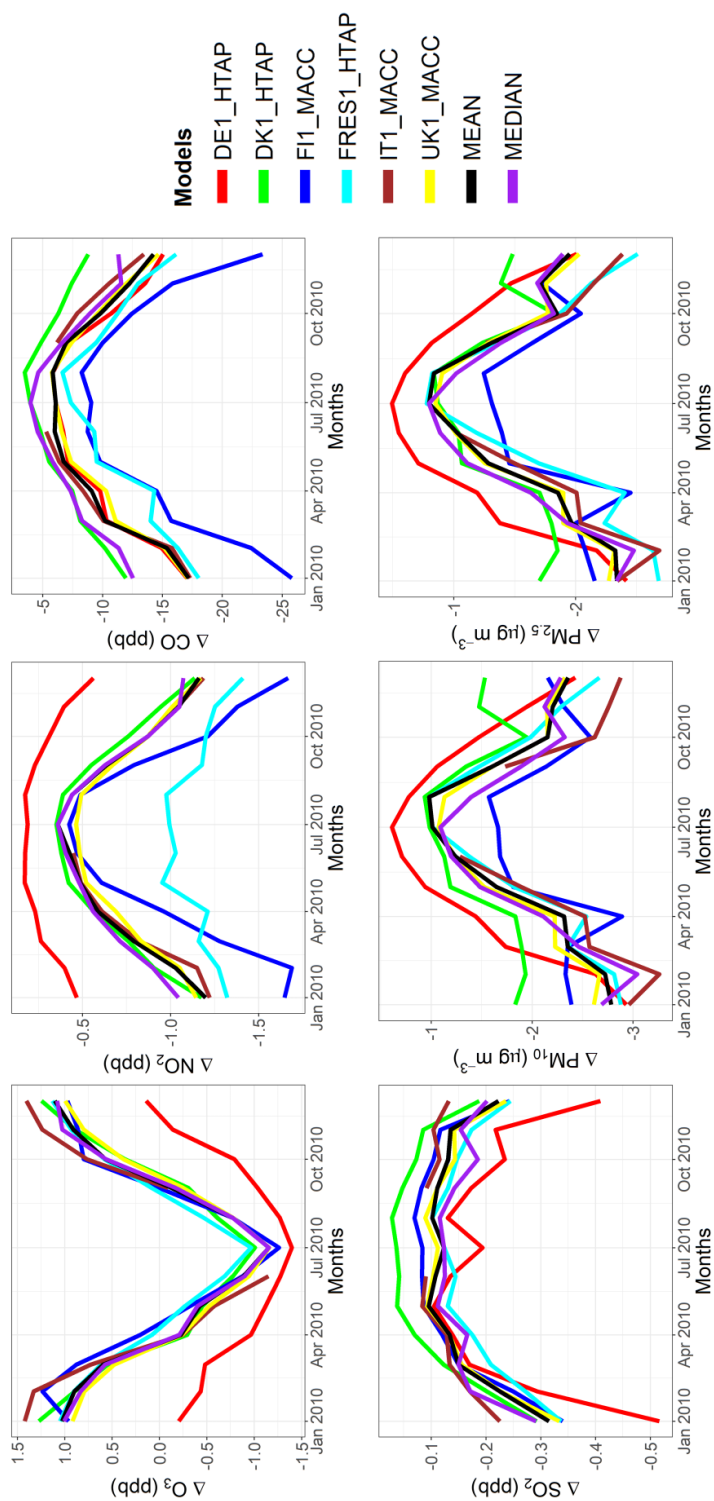
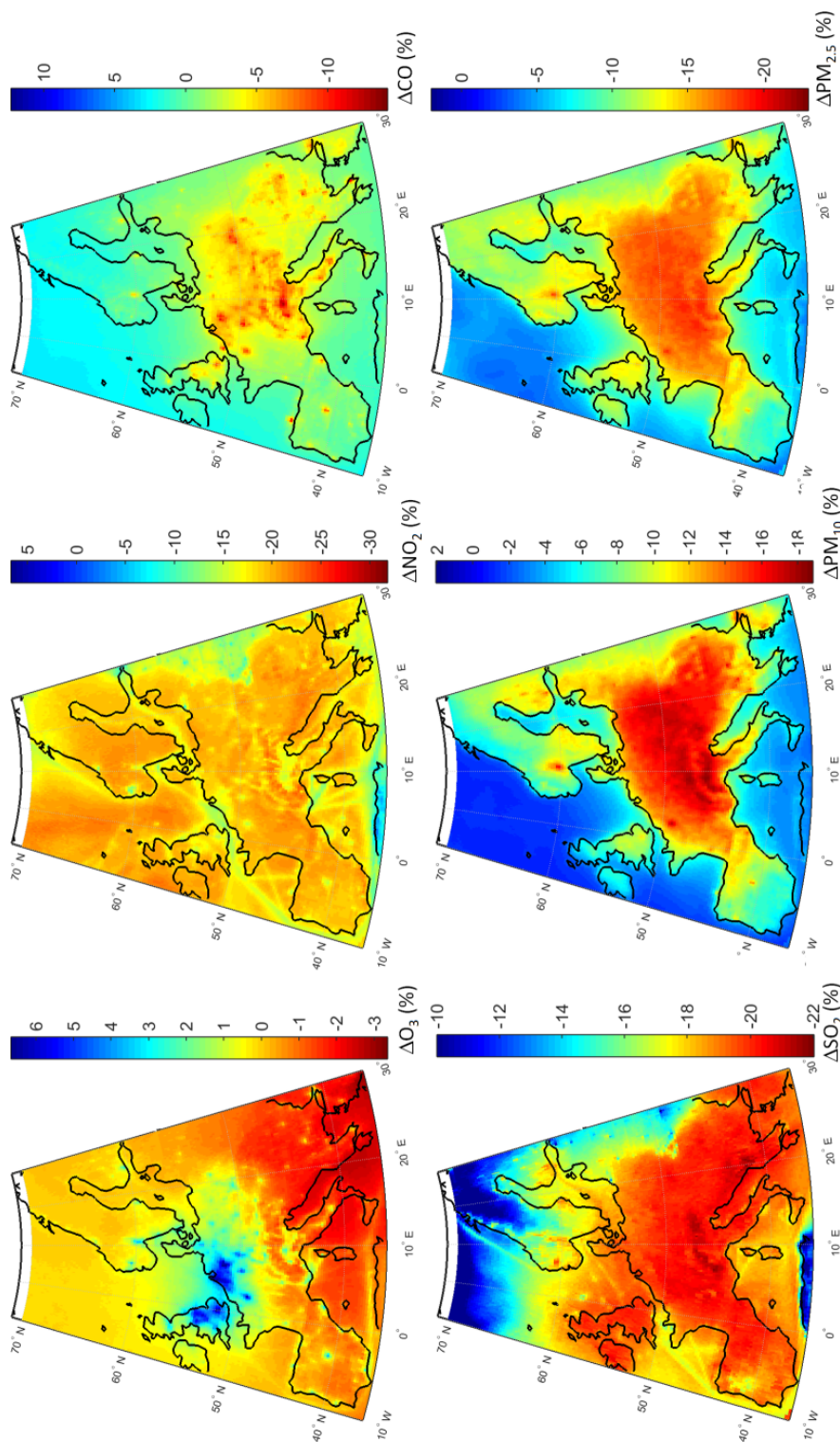


Fig.13. Absolute impact of the 20% reduction of the European anthropogenic emissions over Europe (EUR_{EUR-BASE_EUR}).

890

891
 892

893



894

895 Fig.14. Spatial distribution of the annual mean relative differences between the European emissions perturbation scenario and the base case over

896 Europe as simulated by the multi-model mean ensemble.

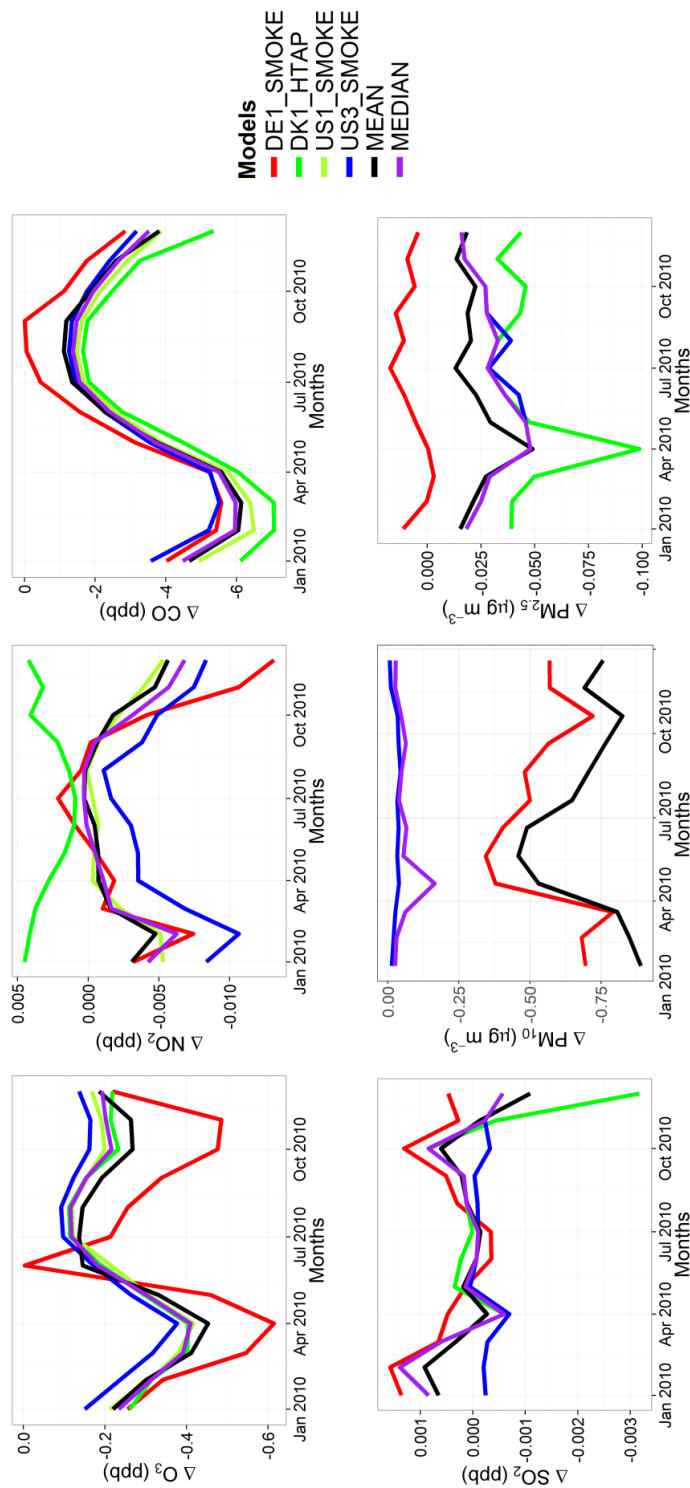


Fig. 15. Absolute impact of the 20% reduction of the East Asian anthropogenic emissions over North America (GLO_{NAM}-BASE_{NAM}).

897

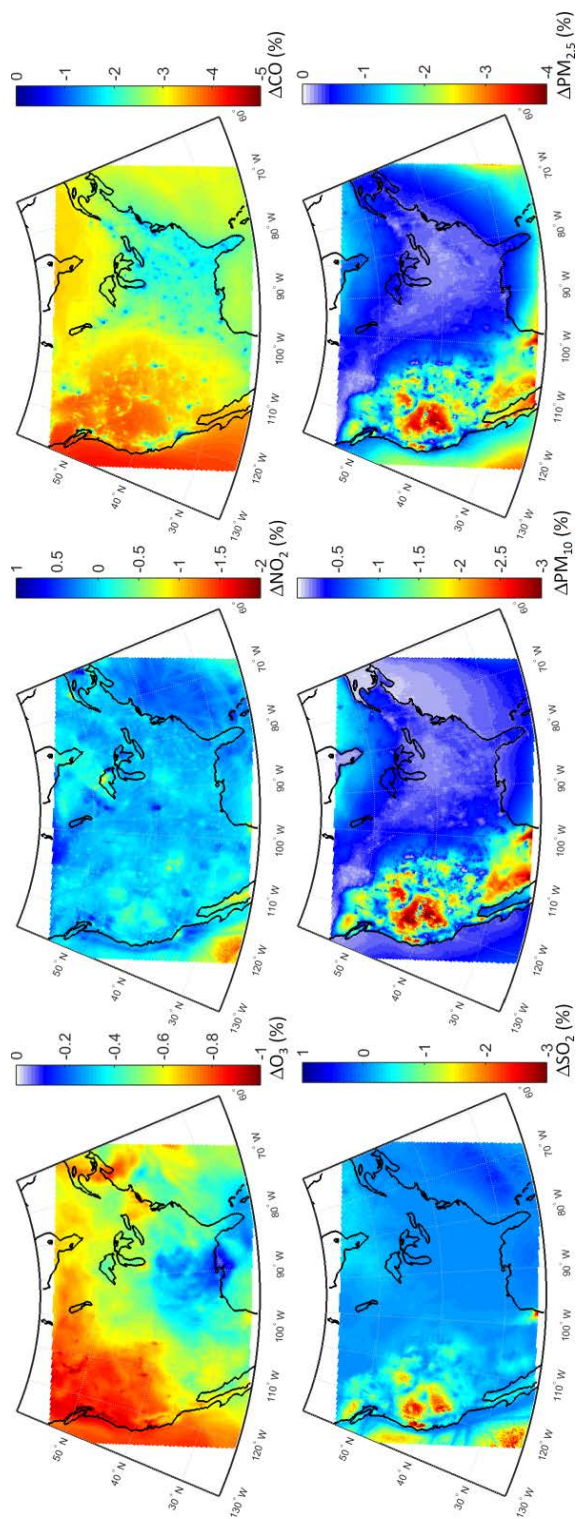
898

899

900

901

902



903

904 Fig. 16. Spatial distribution of the annual mean relative differences between the East Asian emissions perturbation scenario and the base case
905 over North America as simulated by the multi-model mean ensemble.